Title
Drug Transport Across Ocular Epithelial Tissue Using Micro, Nano and Surface Modified Polymer Devices

Author
Wade, Jennifer Simone

Publication Date
2014

Peer reviewed|Thesis/dissertation

Drug Transport Across Ocular Epithelial Tissue Using Micro, Nano and Surface Modified Polymer Devices

by

Jennifer Simone Wade

DISSERTATION

Submitted in partial satisfaction of the requirements for the degree of

DOCTOR OF PHILOSOPHY

in

Bioengineering

in the

GRADUATE DIVISION

of the

UNIVERSITY OF CALIFORNIA, SAN FRANCISCO

AND

UNIVERSITY OF CALIFORNIA, BERKELEY

[redacted]

ACKNOWLEDGEMENTS

Thank you to my advisor, Professor Tejal A. Desai, for her guidance, scientific expertise, flexibility, patience and encouragement. I am sincerely grateful for the opportunity to explore my scientific and entrepreneurial interests under her tutelage.

I am extremely appreciative of the support, guidance and encouragement provided by my committee members Professor Dorian Liepmann and Professor Deanna Kroetz. Their insight and overall contribution to my growth as a scientist has been invaluable.

Thank you to the members of the Desai Laboratory past and present. The culture of curiosity, inclusion and collaboration that you create is what makes this lab great. Honorable mention to Lalitha, Hari & Kelly whom I cannot thank enough for the lessons they've taught me. Additional thanks are also happily given to the following lab members for their contributions to the experiments in this manuscript: Jessica Allen, James Pinney, Crystal Nyitray, Alec Cerchiari and Kevin Lance.

For their support throughout this (longer than anticipated-lol) journey I am forever grateful to the members of Prep for Prep 9 Contingent V, ORDP Alpha & Beta, BGESS and the 2LWC.

I would never have embarked upon this journey nor made the decision to return without the counsel of Mrs. Monika Moo-Young, Dr. Horace K. Moo-Young, Dr. Ann Daugherty and Dr. Osi Esue. Thank you!

To Aunt Lee and my enormous family thank you for celebrating all of my academic achievements. It takes a village!

To Peter, no location exists in this universe nor an alternate one where I could have completed this degree without your support. Koszonom szepen es nagyon szeretlek teged!

To my big brother Tony, thanks for always helping me to keep in perspective how far I have travelled and what is of true value when the chips are down. You have done more than your share and I am forever grateful!

Last but not least, thank you Mom! You've been an inspiration, an example and my biggest cheerleader. None of this would be possible were it not for your sacrifices and the lessons you have imparted. Thank you for providing me with the tools to achieve whatever I set my mind to!!

Funding for this work was kindly provided by Genentech, Inc. and the National Institute of Health. Immunofluorescence images were acquired at the Nikon Imaging Center at UCSF. All SEM was performed at the San Francisco State Electron Microscopy Facility. All lamination was performed in the laboratory of Dr. Ronald Fearing at UC Berkeley. I am grateful for the generous donation and guidance on hfRPE cell cultivation provided by Dr. Sheldon Miller and Dr. Arvydas Maminishkis at the National Eye Institute.

ABSTRACT

Ocular disease treatment with pharmaceutical agents poses a unique set of challenges that can be attributed to the distinctive anatomy of the eye. Novel methods to overcome the barriers of the eye to deliver therapeutics are an area of focus for both academic and industrial researchers. In this dissertation, an *in vitro* model of the posterior ocular epithelial barrier was leveraged to characterize drug transport using microfabricated polymer devices. The influence of planar microdevice geometry on macromolecule permeability was investigated. Planar microdevices enhanced the transport of large molecular weight dextrans in a size dependent fashion. This phenomena was initiated by a non-toxic interaction between the microdevices and retinal tight junction proteins, suggesting that increased transport occurs via a paracellular pathway. Chitosan surface modified planar devices did not demonstrate a comparable permeability enhancing effect.

A comparison between supermicro, micro- and nanofiber films was conducted to elucidate the impact device size has on macromolecule drug transport. Our results demonstrated increased permeability, through a paracellular initiated mechanism, in the presence of micro- and nanofiber films but not supermicro fiber films. Further, drug properties such as molecule shape, charge and size demonstrated that they could enhance or diminish transport irrespective of device size. Which provided valuable insight into drug classes that would be best served by this delivery modality. Finally, co-delivery of a therapeutic and verapamil, an efflux pump inhibitor, was investigated as a strategy for enhancing permeability of small molecules. Our results displayed a drug permeability

reduction in the presence of verapamil; suggesting that transporter protein localization as well as inhibitor specificity are important variables for the success of a small molecule co-delivery approach. The aforementioned experiments demonstrate distinct techniques for modulating drug transport across the ocular barrier using microfabricated polymer devices. Further, the observed trends can be used to design enhanced delivery systems for the administration of ocular therapeutics.

Table Of Contents

List Of Figures

Chapter 1: Introduction

1.1 Motivation

Diseases of the anterior and posterior eye impact 14.25 million people globally. A brief list of these diseases includes: Diabetic retinopathy, Glaucoma, Retinal Vein Occlusion, Uveitis, Wet and Dry Age Related Macular Degeneration [1,2]. In each of these diseases the quality of life is dramatically impacted. Failure to treat these ailments causes severe visual impairment and eventually total vision loss. More than 2 million people in the United States are impacted by Age Related Macular Degeneration (AMD) [3]. The initial phases of AMD impact central vision causing difficulty with daily tasks such as reading, writing and cooking. While peripheral vision is initially largely unaffected, in the later stages of AMD total vision loss is common [4].

AMD has been studied extensively with substantial advances being made into understanding the etiology of the condition. High levels of vascular endothelial growth factor (VEGF) have been implicated in the pathology of ocular neovascular disorders such as AMD and Diabetic Retinopathy [5]. This knowledge combined with advances in biotechnology has enabled researchers to design efficacious pharmaceutical treatments [6]. As a result, four anti-VEGF treatments have been gaining traction as the standard of care; specifically Ranibizumab (Lucentis®), Bevacizumab (Avastin®), Pegaptanib (Macugen®) and Aflibercept (Eylea®).

The standard of care for delivery of ocular therapeutics varies from the anterior to posterior section of the eye and with the physiochemical properties of the pharmaceutical agent. Drugs meant for the front of the eye are typically formulated as liquids and administered via eye drops. For the posterior eye many delivery techniques such as systemic, transcleral and suprachoroidal administration have been attempted [7–9]. However, the primary standard of care is direct delivery into the vitreous via injection. Repeated intravitreal injections have been known to cause a variety of complications including endophthalmitis and retinal detachment [10,11]. As a result novel ocular drug delivery approaches are currently being explored.

1.2 Ocular Physiology and Drug Delivery Barriers

The anterior barriers of the eye can be broken into three compartments: the tear film, cornea and conjunctiva. The tear film is the first barrier encountered when attempting to deliver therapeutics to the anterior eye. The turnover of lacrimal fluid prevents substantial drug residence time on the surface of the eye. This results in limited permeability and low bioavailability of the therapeutic [12,13]. The cornea is comprised of five distinct layers; the endothelium, Descemet's membrane, the stroma, Bowman's membrane and the epithelium (Fig. 1.1). Each layer acts as an independent barrier to molecules of different physical properties. As a result therapeutics must be carefully formulated to avoid the transport limiting properties of each layer. Two layers provide the majority of molecule restriction; the epithelium and stroma. Hydrophilic molecules are limited by the corneal epithelium and extremely lipophilic molecules are limited by the stroma. Due to the structure of

these tissues small molecules (< 600 Daltons) which are lipophilic in nature are primarily absorbed via the cornea [14–17]. Finally, the ocular mucous membrane known as the conjunctiva limits transport primarily through the conjunctival epithelium. While an ideal location for the transport of hydrophilic molecules, bioavailability remains low due to systemic circulation losses [18].

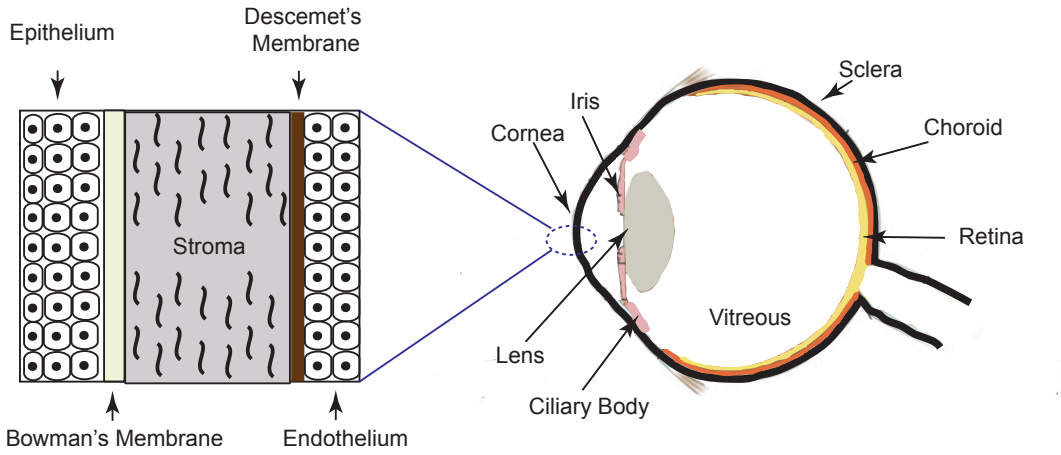

Figure 1.1: Schematic representation of the eye. Exploded section includes detailed view of the five corneal layers.

The posterior eye is separated from the anterior eye by the lens, iris and ciliary body (Fig. 1.2). It is comprised of the vitreous humor, retina, choroid and sclera. The sclera is a thick matrix of collagen and proteoglycans which serves as the outer most layer of the eye. It is an avascular structure of variable thickness comprised of the lamina fuscia, stroma and episclera. It is known to be permeable to macromolecules up to 69 kDa [8,17,19]. The choroid is a highly vascularized network sandwiched between the sclera and retina. It is comprised of the Bruch's Membrane, choriocapillaries, two layers of larger choroidal vessels (Haller's and Sattler's) and the suprachoroid [19–21].

The vitreous is a transparent viscous fluid that influences the shape of the eyeball. It is in direct contact with the retina which is comprised of the inner limiting membrane, nine layers of the neural retina and the retinal pigment epithelium [19,22,23]. Drug transport to the posterior eye is very difficult due to the numerous barriers posed by the anterior segment, sclera, choroid, inner and outer blood retinal barriers.

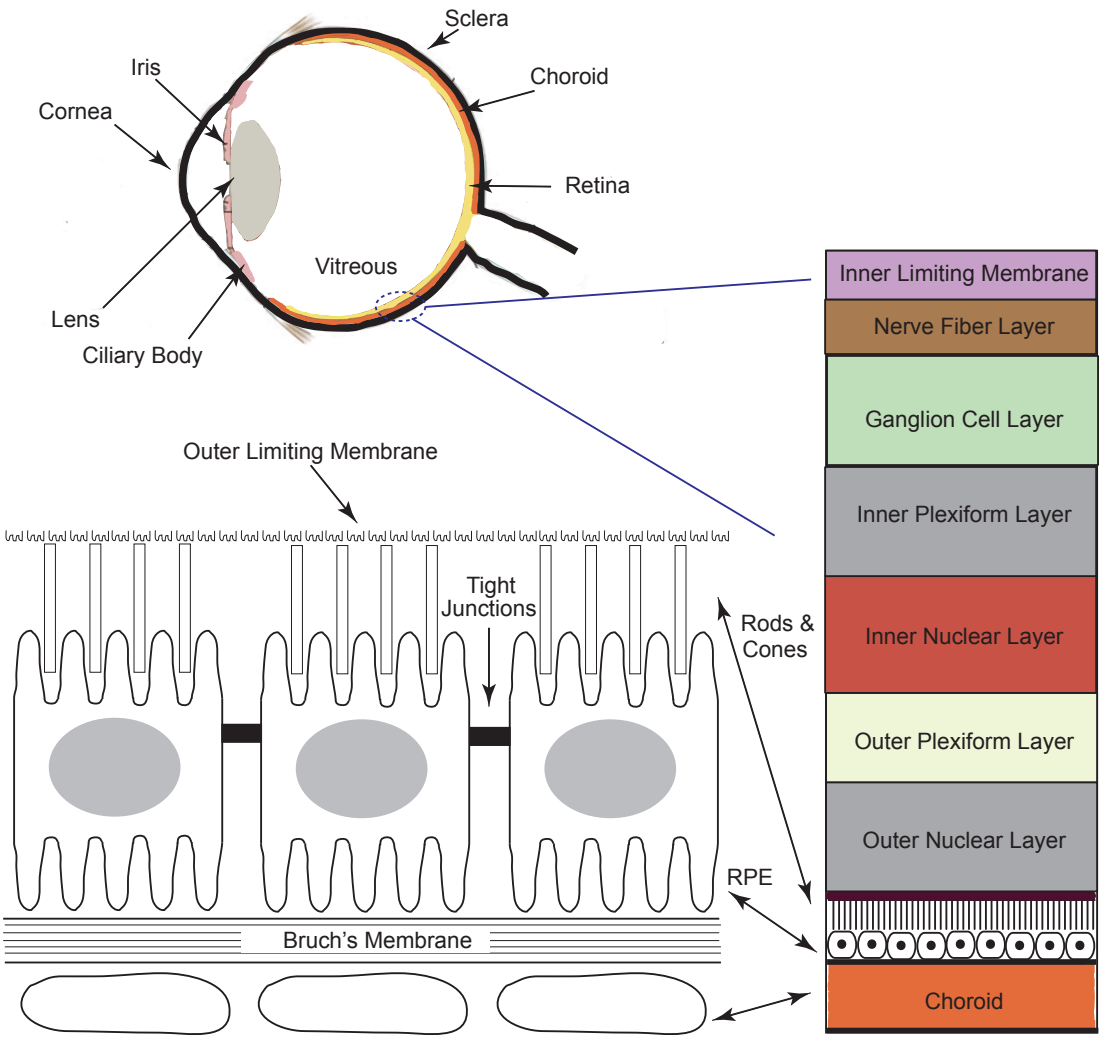

Figure 1.2: Schematic representation of the eye. Exploded section includes detailed view of the neural retina and outer blood retinal barrier.

The inner blood retinal barrier is comprised of tight junctions formed between adjacent endothelial cells. This barrier controls movement of molecules and fluid between retinal tissues and the vascular structure of the eye. The inner blood retinal barrier (iBRB) is also the primary impediment for the transport of macromolecules which are administered systemically [13,18,22]. The outer blood retinal barrier (oBRB) is comprised of tight junctions formed between adjacent epithelial cells of the Retinal Pigment Epithelial (RPE) layer. These tight junctions limit the paracellular movement of molecules between the apical and basolateral sides of the RPE. The basolateral side of the RPE is adjacent to the Bruch's membrane and separates the capillaries of the choroid from the neural retina. The primary role of the RPE is to transport nutrients from the blood to the outer neural retina and absorb scattered light [24]. As such it plays a critical role in ensuring the health and proper function of the retina. It is poorly permeable to large as well as small molecules and has an extensive transporter network to selectively confer passage of molecules between the apical and basolateral sides [25–27].

Transport of drugs through ocular tissues occurs via transcellular or paracellular transport. Transcellular transport occurs as molecules move across the cellular membrane via one of three mechanisms: passive diffusion, carrier mediated transport, and endocytic processes [28,29]. Passive transcellular diffusion is the dominant transport route for lipophilic low molecular weight therapeutics and is driven by the concentration gradient across the cell. Carrier mediated transport leverages membrane transport proteins to shuttle substrates across the cell layer irrespective of

the concentration gradient [28,29]. This method of transport is commonly used by small molecules that are less than 500 Daltons [28]. Endocytosis is the dominant transcellular transport route for large molecular weight therapeutics however it is a highly saturable process.

Carrier mediated transport is dependent on the quantity of transporters in the cell membrane and the affinity between the therapeutic and transporters. Transporters serve an important role in various tissues and are responsible for the movement of a plethora of substrates including xenobiotics, nutrients and waste [19]. Transporters have been extensively studied in the major organs associated with first pass metabolism, biliary and renal elimination. However the prevalence and role of transporters in ocular transport has only recently been investigated. Amino acid transporters such as SLC7, SLC6 and the SLC1 glutamate transporter family have been identified in several retinal pigment epithelial cell lines [18]. Of interest is the variability in expression and behavior of these well-studied transporters in ocular cell models, such as the absence of oligopeptide transporters (e.g. SLC15) that have been implicated in the transport of many xenobiotics. Further, organic cation transporter substrates such as the glaucoma therapeutic brimonidine, have displayed atypical kinetics *in vitro* and *in vivo* suggesting that transporters in the retina may have different or overlapping mechanisms [18,30]. This is of grave importance as several small molecule ocular therapeutics are substrates for the aforementioned transporters [18,25,31].

Endocytosis is believed to be the primary cellular internalization mechanism for macromolecules. Phagocytosis and pinocytosis are two sub-classifications of the endocytic transport process. Phagocytosis is performed by specialized cells therefore it is an unlikely retinal epithelial transport mechanism. Conversely with pinocytosis, large molecules can either bind to a specific membrane receptor or to a non-specific membrane receptor [28,32]. The membrane then forms an invagination and inward channel to internalize the molecule and provide a pathway for the macromolecule to travel out of the cell. These processes are called receptor mediated, absorptive or fluid-phase pinocytosis. While some macromolecules are internalized by pinocytosis there is always the risk that their structure will be disrupted by lysosomes prior to being released on the basolateral side of the epithelial barrier [28,32,33]. As a result it is more likely that macromolecules which are successfully transported transcellularly use a receptor-mediated endocytosis or transcytosis process. These pathways are still being investigated but to date transferrin, FcRN, Caveolin-1 and Clathrin mediated endocytosis have been implicated in ocular transport [32–34].

Paracellular transport occurs as molecules move between adjacent cells that are secured to each other through tight junction proteins, adherens junctions and desmosomes [35]. This pathway is the dominant route for hydrophilic small molecules and large molecules that have a hydrodynamic radius smaller than 5 nanometers [33,36–38]. Electron microscopy conducted by numerous groups has concluded that tight junctions are an interlaced arrangement of focal contacts between the plasma membranes of neighboring cells [23,35,39]. Tight junctions are

comprised of claudins, occludins and junctional adhesion molecules (JAM). Zonula occludens are often classified as tight junction proteins however, they behave more like linkers between occludin and the filaments of actin found in the cytoskeleton [40,41]. There are numerous subtypes of tight junction proteins; to date twenty-four have been identified just for claudin [41,42]. However, protein expression and function varies between epithelial cell lines. Certain epithelial cell lines exhibit more characteristics of permeability than others based on the subtype and subtype ratio of tight junction proteins expressed [43,44]. Research has shown that paracellular transport can be regulated by manipulation of the tight junction proteins [40,45]. It is believed that cellular signaling mechanisms influence tight junction behavior but this is still an area that is being actively investigated [46].

The physiochemical properties of a therapeutic play a significant role in influencing the dominant transport mechanism of a drug across or between cells. Some examples of these properties include lipid solubility, partition coefficient, drug ionization, molecular weight, aqueous solubility and chemical stability [47,48]. These physical properties are also a key determinant of the rate of passive paracellular drug permeation.

While advances have been made in our understanding of ocular pharmacokinetics of small and large molecules, the influence of drug delivery devices, and biomaterial architecture has not been extensively studied. In this work, human retinal pigment epithelial (RPE) cell models were used to explore the mechanisms of small and

macromolecule transport when encapsulated in microscale planar devices (Chapters 2 & 5), delivered in the presence of surface modified microdevices (Chapter 3), or delivered using micro- and nanotopography (Chapter 4).

Chapter 2: Planar Microdevices for Large Molecule Transport Across Retinal Pigment Epithelial Cells

2.1 Background

Age-related macular degeneration, a disease of the posterior eye, is the leading cause of vision loss in adults over the age of 60 in developed nations [3]. In the United States, the number of people affected by this disease exceeds 2 million and is expected to double by the year 2020 due to the aging baby boomer population [3]. Recent advances in the biotechnology industry have provided patients with highly effective monoclonal antibody and antibody fragment treatments, such as Ranibizumab, for this debilitating disease.

Ocular administration of therapeutics is one of the greatest challenges in the field of drug delivery due to the numerous barriers protecting the eye. The standard of care for ocular drug delivery is topical application of liquids or gels. However, this method of administration is not effective in delivering large molecules to the posterior segment of the eye. The limited contact time, distance and limited permeability between the anterior and posterior segments lead to poor absorption and correspondingly low bioavailability of the therapeutic [11–14,31,49]. Additionally, the tight junctions of the retinal pigment epithelium (RPE) and endothelial cells make intravenous delivery of large molecules unrealistic. While low bioavailability at the site of action is a primary concern, off-target effects such as toxicity are also a deterrent to this mode of delivery. As a result, the primary treatment employed to address posterior segment diseases is intravitreal injection

[11]. This highly invasive method can cause complications if conducted erroneously and often results in a lack of patient compliance.

A variety of alternative therapies have been developed to address these challenges; they include implantable drug reservoirs, which must be surgically removed, as well as biodegradable microspheres and thermo-responsive gels to sustain therapeutic drug levels in the eye [11,27,50–54]. In addition, several approaches have examined methods to facilitate the permeability of drugs across cellular barriers, including nanoparticles and permeation enhancers. For example, previous studies in rabbits demonstrated that drug uptake in the cornea is enhanced when nanoparticles with a chitosan coating are employed to deliver a small molecule [55–58]. Researchers have begun to incorporate our existing knowledge of retinal physiology to improve drug delivery [59,60]. Recent studies have increased the transport of small molecule drugs by using newly discovered retinal membrane transporters [61–63]. Receptor-mediated endocytosis has been investigated for the transport of large molecules leveraging the recently discovered neonatal Fc receptor (FcRN) and transferrin receptor [33,34,64–69]. Unfortunately, these approaches are highly dependent on molecular structure. For example Ranibizumab, an antibody fragment, will not be internalized via FcRN endocytosis due to its missing Fc region [70,71].

Interest in disrupting barrier function has led to the use of small interfering RNA (siRNA) to target the tight junction proteins claudin and occludin [39,72,73]. However, use of siRNA *in vivo* is contentious due to concerns about the efficiency of intracellular

delivery, reversibility and off-target effects. To date, the effect of device architecture to modulate the retinal barrier, for large molecule drug transport, has not been investigated.

Using established microfabrication techniques, we have developed SU-8/ Poly(ethyleneglycol)dimethacrylate (PEGDMA) planar microdevices, which maximize contact surface area, provide consistent drug volumes and can be used to unidirectionally deliver large molecule therapeutics. SU-8 was chosen because it is a well-characterized negative photoresist that can easily be patterned into complex structures with specific dimensions [74,75]. PEGDMA is a biocompatible and commonly used hydrogel, which permits the safe encapsulation of a therapeutic and tunable release in the presence of an aqueous solution [76–80].

These devices have previously been successful in delivering small molecules across an intestinal epithelial cell line, specifically human colorectal adenocarcinoma (Caco-2) epithelial cells [81–84]. In this work, we extend our research to the delivery of large molecules across two human retinal pigment epithelial cell types, an adult retinal epithelial cell line (ARPE-19) and fetal retinal epithelial primary cells (hfRPE). ARPE-19 cells have been extensively studied, demonstrate *in vivo* physiological characteristics of retinal tissue, and can be both easily acquired and cultured [85–87]. When compared to the broader set of spontaneously immortalized human retinal epithelial cell lines, it is the preferred choice for the aforementioned reasons. However, previous studies have demonstrated that primary cell lines retain more morphological and physiological characteristics than spontaneously immortalized cell lines [87]. For this reason a primary

culture of hfRPE cells were used to generate an understanding of how well the results from these transport studies would translate to an *in vivo* model. Both types of cells are established and accepted, *in vitro* models for retinal drug delivery.

2.2 Materials & Methods

2.2.1 Materials:

ARPE-19 cells were obtained from American Type Culture Collection (ATCC) and human fetal retinal pigment epithelial cells (hfRPE) were kindly donated by the National Eye Institute laboratory of Sheldon Miller Ph.D. Dulbecco's modified eagle medium (DMEM:F12 [1:1]) for cell culture, Fetal Bovine Serum, Penicillin-streptomycin antibiotic solution, PBS and mouse laminin were obtained from the UCSF Cell Culture Facility. Fetal Bovine Serum for the hfRPE cells was obtained from Atlanta Biologicals and all remaining media components were obtained from Sigma-Aldrich [87]. Transwell inserts and FITC dextran spanning molecular weights of 4 to 150 kDa were obtained from Sigma-Aldrich. The hydrogel precursor solution, comprised of PEGDMA (750 mol. wt.), dimethoxy-phenyl acetophenone (DMPA) and polyvinylpyrrolidone (PVP) was purchased from Sigma-Aldrich. The SU-8 photoresist was purchased from Microchem (Newton, MA).

2.2.2 Cell Culture:

The ARPE-19 cell line was derived from the normal eyes of a 19 year-old male. The cells were grown in a T-75 flask with a 1:1 mixture of DMEM:F12 high glucose media containing 10% Fetal Bovine Serum (FBS) and 1% Penicillin-streptomycin antibiotic

solution. The *in vitro* retinal model was constructed using a 24-well, high density 0.4μm transwell filter insert and plate assembly. The transwell filter inserts were coated with a 1:10 mouse laminin-DMEM:F12 serum free mixture and allowed to dry overnight in a cell culture hood. The ARPE-19 cells were seeded on the filters at a density of 4.5×10^5 per insert. The media used for the transwell inserts is the same as described above with the exception of the fetal bovine serum, which is added at 1% of the total volume. All cells were maintained at 37°C in 5% CO_2. ARPE-19 cells were used between passages 25 and 35.

Passage 0 flasks were provided with hfRPE cells derived from the eyes of a 16-18 weeks of gestation fetal donor. Briefly, the cells were grown in a T-75 flask with a Minimal Essential Medium-Alpha (MEM-α) mixture of media containing 5% heat inactivated FBS, N1 supplement (1:100 mL/mL), glutamine-penicillin-streptomycin (1:100 mL/mL), nonessential amino acid solution (1:100 mL/mL), hydrocortisone (20 μg/L), taurine (250 mg/L) and triiodo-thyronin (0.013μg/L) [87]. The *in vitro* retinal model was constructed using a 24-well, high density 0.4μm transwell filter insert and plate assembly. The transwell filter inserts were coated with a human extracellular matrix from human placenta in serum free MEM-α media, UV cured for 2 hours and allowed to dry overnight in a cell culture hood. The hfRPE cells were seeded on the filters at a density of 40×10^4 per insert. All cells were maintained at 37°C in 5% CO_2. The hfRPE cells were seeded onto the inserts at passage 1 and were grown to confluence over a 6-8 week period.

2.2.3 Device Fabrication:

The body of the microdevice was fabricated as previously described [81,82]. Briefly, SU-8 was spun onto a silicon wafer and a reservoir was patterned using a two-mask photolithography process. After removal of residual photoresist with an SU-8 developer the wafer was cleaned thrice with deionized water followed by an isopropanol rinse. The wafer was then blown dry with nitrogen and baked for 2 minutes at 95°C to remove all impurities. A hydrogel solution of PEGDMA (750 mol. wt.; 2 mL) was mixed with the photoinitiator dimethoxy-phenyl acetophenone (DMPA; 200 µL of 60 mg/mL) in monomer polyvinylpyrrolidone (PVP). FITC conjugated dextran (200 µL of 20 mg/mL) of varying molecular weights was mixed with the hydrogel solution. This solution was then spun onto the SU-8 microdevice and exposed to UV-light to cross-link the hydrogel in the device reservoir.

2.2.4 Transport Studies:

ARPE-19 and hfRPE cells were grown to confluency on porous transwell filter inserts in a 24-well plate. Confluency was measured using transepithelial electrical resistance (TEER). All transport studies were conducted on cells grown for four to eight weeks on transwell filter inserts. Equal concentrations (13 µg/mL) of the desired therapeutic (4, 40 and 150 kDa FITC dextran) were deposited in the apical chamber of the transwell filter in one of three forms: a standard bolus, a hydrogel bolus, or a planar microdevice. Cells alone and empty planar microdevices were used as controls. At periodic time points the entire volume of the basolateral chamber was removed and replaced with fresh Phosphate Buffered Saline (PBS). The samples were then probed for the concentration of FITC

dextran, transferred to the basolateral chamber, using a fluorimeter. Prior to commencement of the transport studies the inserts were washed two times in PBS and transferred to a new 24-well plate. The media was replaced with phenol red free DMEM: F12 to prevent interference with the fluorimeter measurements.

2.2.5 Analytical Techniques:

The confluency of the ARPE-19 and hfRPE cells was measured using the World Precision Instruments transepithelial electrical resistance (TEER) device. Measurements were taken weekly until confluency was reached at approximately four and six weeks for ARPE-19 and hfRPE respectively. The concentration of FITC-conjugated agents released from the microdevice was measured with a Packard FluoroCount fluorimeter.

2.2.6 Immunofluorescence:

ARPE-19 and hfRPE cells on transwell filter inserts were stained for the tight junction protein zonula occludens-1 (ZO-1) immediately after the conclusion of the permeability studies. The cells were fixed for 30 minutes in 4% formaldehyde-PBS solution at 4°C and washed three times with PBS. The cells were then permeabilized and blocked overnight with a 1% BSA- 0.1% Triton X solution. A ZO-1 rabbit polyclonal antibody (Invitrogen) was diluted 1:100 in blocking solution and incubated with the samples overnight at 4°C. After washing three times with PBS an Alexa Fluor secondary antibody (Invitrogen) was incubated for 1 hour at 4°C. The samples were then mounted for spinning disk confocal imaging.

2.2.7 qPCR for ZO-1, Occludin and MRP-1 Expression:

Cell lysis, reverse transcription and quantitative polymerase chain reaction (qPCR) were performed using the Fast SYBR Green kit as outlined in the manufacturers instructions. Lysis was conducted within one hour post conclusion of the transport studies. The experiments were performed with three biological replicates (n=3) and mRNA expression was probed with three technical replicates for each respective biological replicate. The expression of GAPDH (forward 5'CTCTCTGCTCCTCCTGTTCG-3', reverse 5'GCCCAATACGACCAAATCC-3'), ZO-1 (forward 5'TGTGAGTCCTTCAGCTGTGG-3', reverse 5'TTTCCTGCTCAACTCCTTCG-3'), Occludin (forward 5'ACCGAATCATTATGCACCAAG-3', reverse 5'AGATGGCAATGCACATCACAA-3') and MRP-1 (forward 5'CTGTTTTGTTTTCGGGTTCC-3', reverse 5'GATGGTGGACTGGATGAGGT-3') was analyzed using the specified primer sequences. The results were normalized to GAPDH transcript levels in untreated cells using the ΔΔCt method.

2.2.8 MTT Assay:

ARPE-19 and hfRPE cells were seeded at a density per well of 5 x 10^3 cells in a 96-well plate. The cells were allowed to grow for 48 hours in standard culture conditions. Both cell types were then incubated at 37°C and 5% CO_2 with and without SU-8/PEGDMA planar microdevices for 24 hours. Post incubation the cells were washed thrice with PBS to remove the planar devices. The cells were then allowed to recover for 24 hours in standard culture conditions using phenol red free media. Post recovery 20 µl of MTT solution was added to each well and incubated at 37°C for 4 hours. A volume of 200 µl

of sodium dodecyl sulfate (SDS) solubilization solution was added to the inserts post incubation. Sample absorbance was measured spectrophotometrically at 570 nm and again at 690 nm to account for the background absorbance of the 96-well plate.

2.2.9 Statistical Analysis:

Data are reported as average values plus or minus standard deviation. All data sets were analyzed with a single factor analysis of variance (ANOVA) test followed by the Student t-test. P-values of less than 0.05 were considered statistically significant unless explicitly stated otherwise.

2.3 Results & Discussion

2.3.1 Device Characterization:

Planar microdevices made with an SU-8 base and a poly(ethyleneglycol)dimethacrylate (PEGDMA) reservoir were fabricated using standard photolithography methods as outlined in figure 2.1a. As displayed in figure 2.1b, we successfully created the desired device geometry of a 150 x 150 μm base and 70 x 70 μm reservoir. We then used profilometry to verify the depth of the device reservoir and confirm that photoresist which was not crosslinked was successfully removed during the development process. Based on the desired drug loading concentration the reservoir depth was tuned to 40 micrometers as confirmed using scanning electron microscopy (Fig. 2.S1).

Using the photolithography process flow outlined in figure 2.1c, FITC dextrans with a molecular weight ranging 4, 40 and 150 kDa were incorporated into a PEGDMA and

photoinitiator mixture. The SU-8 patterned silicon wafer was then coated with the aforementioned hydrogel mixture using spin coating, and crosslinked in the 70 x 70 µm device reservoirs as depicted in figure 2.1c. Figure 2.1d demonstrates the successful encapsulation of the FITC labeled dextran. Corresponding elution studies confirmed that FITC dextran could be released from the devices over a four-hour period when placed in an aqueous solution (Fig. 2.S2).

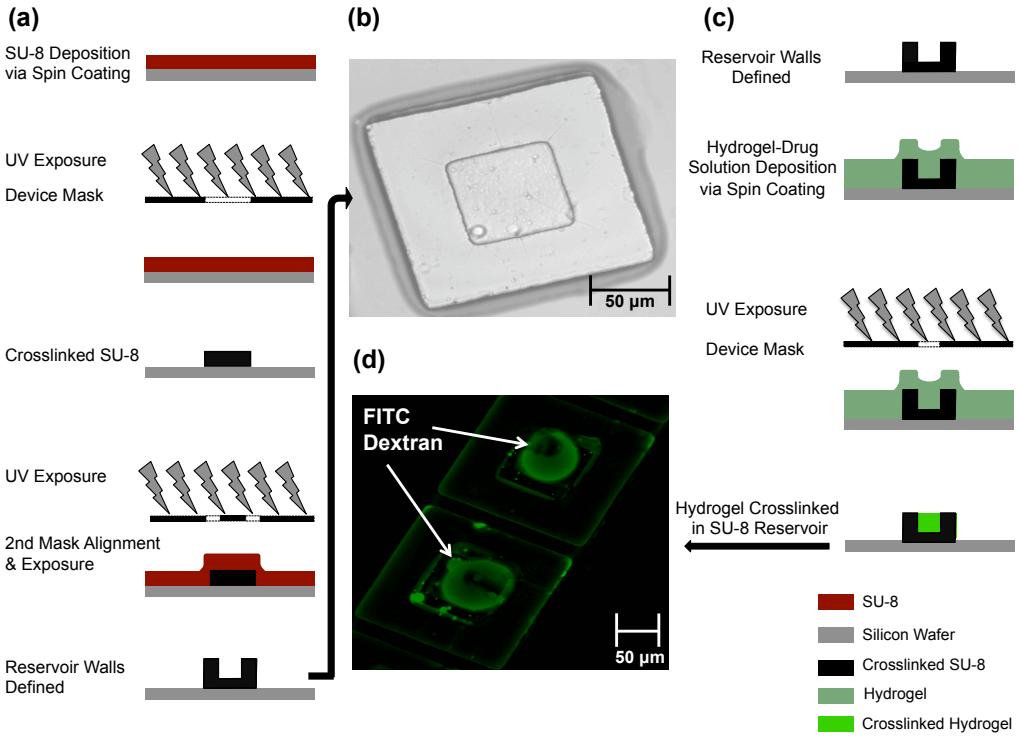

Figure 2.1 SU-8 Device Fabrication Process and PEGDMA Hydrogel Encapsulation. (a) Schematic representation of fabrication using standard photolithography and a two-mask process to generate a reservoir structure. (b) Bright field image of SU-8 device with defined features. (c) Schematic representation of PEGDMA Hydrogel being crosslinked in the device reservoir (d) Image of encapsulated FITC conjugated drug [4 kDa dextran].

2.3.2 Cell Viability:

The devices were incubated on the two types of retinal pigment epithelial (RPE) cells for twelve hours and cell viability was determined with the colorimetric MTT assay. ARPE-19 and hfRPE cells not exposed to planar microdevices were used as the control. The results suggested that the devices were not toxic to the cells (Fig. 2.2a, b). This was also confirmed via cell imaging of the ZO-1 tight junctions both with and without the presence of a device. In the absence of a device the cellular tight junctions were continuous and displayed no signs of disruption (Fig. 2.2c). Upon comparison to the stained cells in the presence of an empty planar microdevice one could see no significant difference in cell morphology (Fig. 2.2d). This supports the assertion that these devices were not toxic to RPE cells and that an adverse cellular reaction was not the cause of the increased transport witnessed in the presence of the planar microdevices.

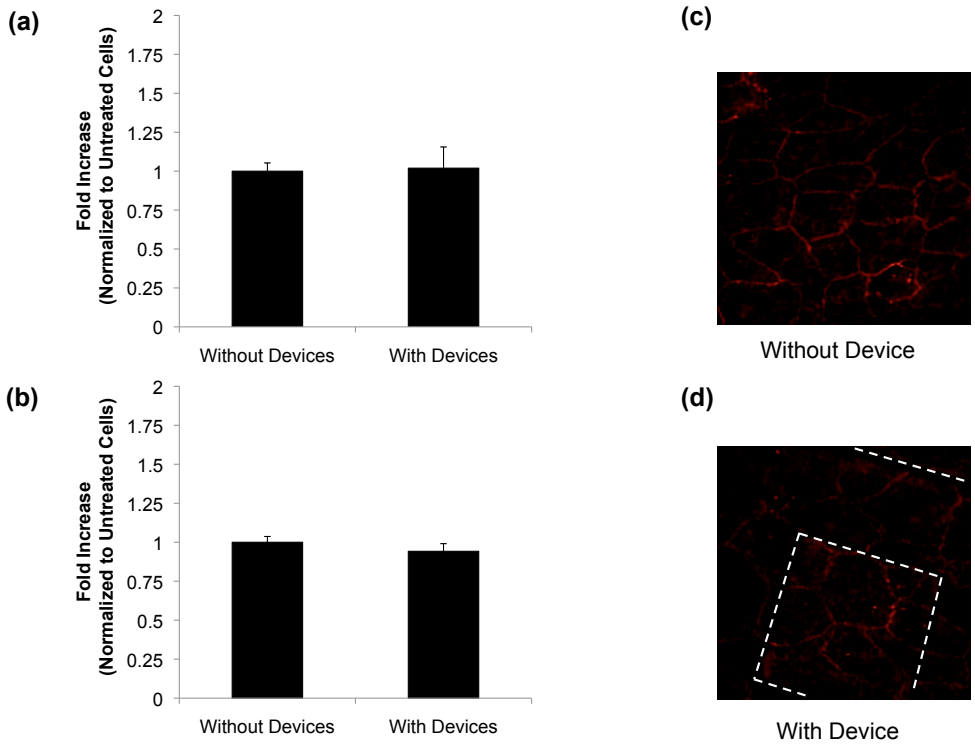

Figure 2.2 MTT Assay. MTT assay of (a) ARPE-19 and (b) hfRPE incubation with and without devices confirms cell viability. ARPE-19 zonula occludens 1 (ZO-1) staining confirms formation of tight junctions (c) without devices and (d) with devices. All data is presented as +/- standard deviation. An asterisk (*) indicates statistical significance with respect to the untreated cells with a P-value of less than 0.05.

2.3.3 FITC Dextran Transport Studies in ARPE-19:

Figure 2.3 presents a schematic representation of the permeability studies experimental setup. A transwell insert with a porous membrane has been placed into a receiving chamber. The apical chamber is clearly separated from the basolateral chamber by the monolayer of retinal pigment epithelial cells (RPE). However the porous membrane, which supports the RPE cells, will permit molecules that traverse the epithelial layer to move into the basolateral chamber. In figure 2.3a, the apical chamber is filled with a

traditional bolus of FITC dextran. This bolus was deposited using a micropipette. In figure 2.3b, the apical chamber is filled with FITC dextran loaded planar microdevices. The devices are removed from the wafer using a sterile razor and suspended in PBS. They are then deposited in the apical chamber using a micropipette where they settle onto the epithelial cell layer. The asymmetric design of the devices facilitates a higher concentration of FITC dextran at the epithelial cell surface.

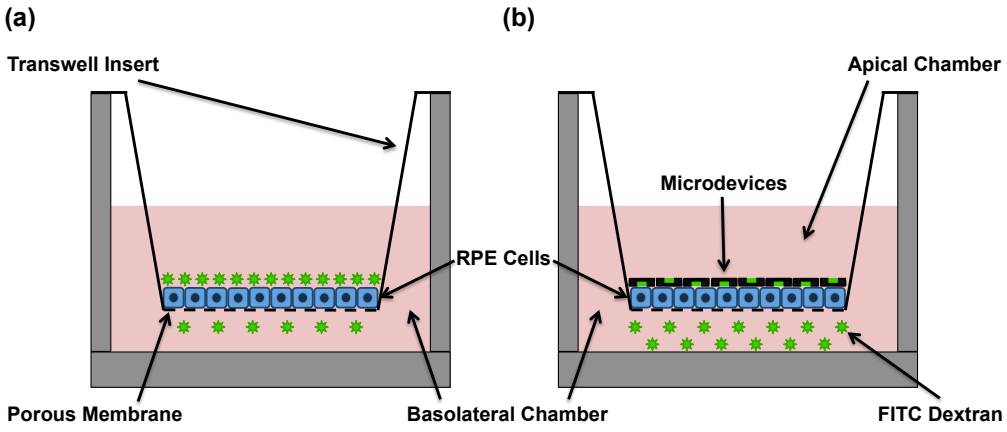

Figure 2.3 Permeability Studies Experimental Setup. (a) Schematic representation of a transwell insert with bolus drug being deposited in the apical chamber. (b) Schematic representation of drug loaded SU-8/PEGDMA planar microdevices being deposited in the apical chamber of a transwell insert.

Permeability studies using FITC dextran were conducted across a monolayer of ARPE-19 cells which were grown to confluence on the apical side of high density porous transwell inserts (qty:24, n=4) over a period of 4 to 6 weeks. These adult retinal pigment epithelial cells (ARPE-19) are the accepted *in vitro* model of the retinal epithelium [85,86]. The transport studies conducted across a monolayer of ARPE-19 cells suggested that

encapsulation of FITC dextran in the planar microdevice significantly enhanced its transport compared to the traditional bolus drug deposition alone. This trend was observed for 4 kDa, 40 kDa and 150 kDa FITC dextran samples (Fig. 2.4a, b, c). As expected, the amount of FITC dextran transported across the monolayer of ARPE-19 cells decreased as molecular weight increased (Fig. 2.4d). These data suggest that planar microdevices could be of value for the delivery of biologics/proteins, which span a range of sizes, such as Insulin (6 kDa) to Bevacizumab (149 kDa). The planar architecture, unidirectional elution and increased contact time between the device and RPE cells likely contributed to the enhanced transport. Additionally, the difference in FITC dextran transported, between the device and the bolus, decreased with increasing molecular weight. This observation led us to conclude, that while these devices could be used to transport high molecular weight therapeutics, there is an upper size limit for the optimal transport effect. Additionally, this upper limit could be attributed to the hydrogel mesh size. It is well established that variations in polymer molecular weight as well as polymer and photoinitiator concentration have a direct impact on hydrogel mesh size [51]. As a result all devices were made with PEGDMA of a single molecular weight and consistent concentrations. The mesh size of the crosslinked hydrogel is 6 to 20 nanometers in a dehydrated state. The hydrodynamic radii of the FITC dextrans used in this manuscript are 1.4, 4.5 and 8.5 nanometers and correspond to 4, 40 and 150 kDa FITC dextran respectively. The mesh size is large enough to permit diffusion of the three types of dextrans in a swollen state. However, the ratio of mesh size to hydrodynamic radius was not designed to remain constant with the increasing molecular weight of the FITC dextrans. Thus the rate of transport reduction, with increasing payload molecular weight,

could also be attributed to the three distinct ratios of pore size to dextran hydrodynamic radius.

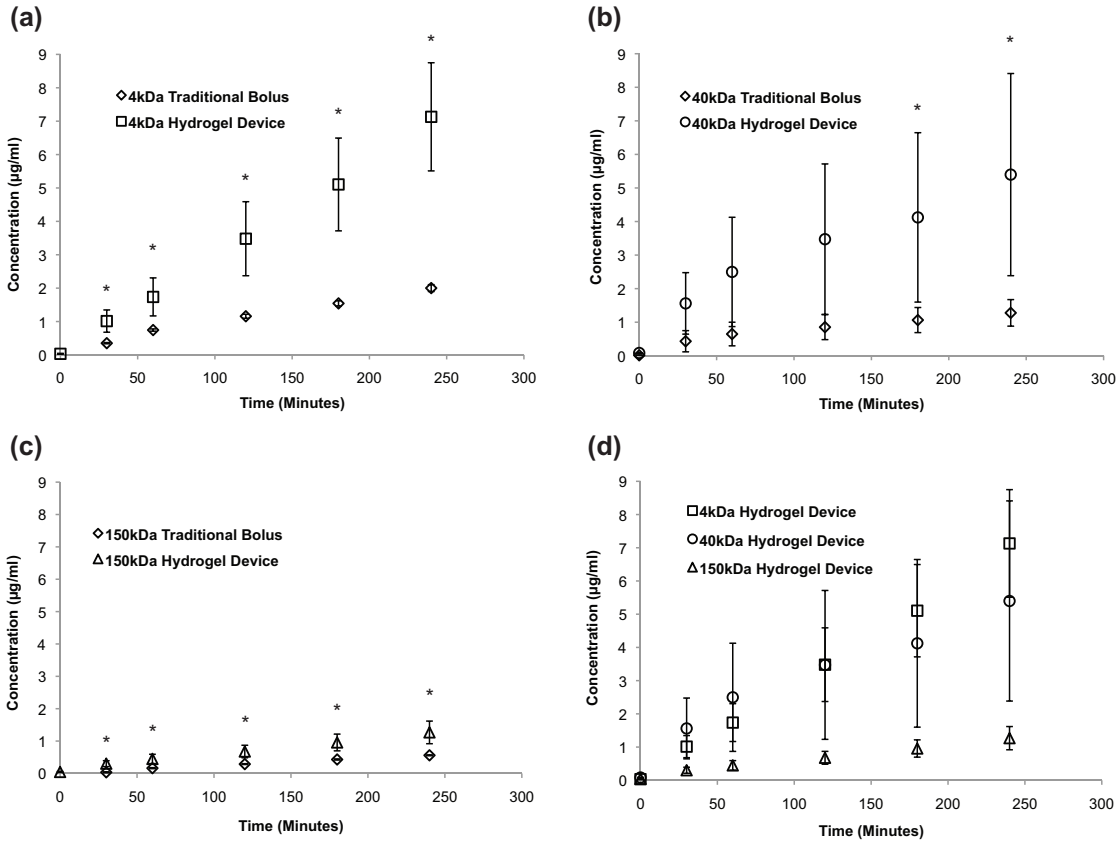

Figure 2.4 ARPE-19 Permeability Studies. Transport of FITC dextran across a monolayer of ARPE-19 cells grown on transwell inserts using a traditional bolus and planar hydrogel devices. FITC dextran of varying molecular weights (a) 4 kDa, (b) 40 kDa, (c) 150 kDa was deposited in the apical chamber and encapsulated in planar SU-8/PEDGMA devices for each experiment. (d) The concentration of drug transported is molecular weight dependent. An asterisk (*) indicates statistical significance with respect to the traditional bolus conditions. All data is presented as +/- standard deviation.

2.3.4 FITC Dextran Transport Studies in Human Fetal Retinal Pigment Epithelium (hfRPE):

While ARPE-19 cells are the accepted model for retinal drug transport due to their ease of acquisition and propagation, we have extended our work to a primary cell line, specifically human fetal retinal pigment epithelial cells (hfRPE). Given the morphological and physiological characteristics of hfRPE's, this culture may better mimic some of the interactions that occur *in vivo* and as such is an appropriate extension of our work. Further this primary culture has been employed to understand how well the results from our transport studies would translate to an *in vivo* model. Passage 1 of the hfRPE cells were grown to confluence on the apical side of high density porous transwell filter inserts (qty: 24, n=4) over a 6 to 8 week period. In the hfRPE experiments we observed the same trend between the hydrogel device and traditional bolus that was seen when delivering FITC dextran across ARPE-19 cells. The hydrogel-loaded microdevices outperformed the traditional bolus in the 4 kDa, 40 kDa and 150 kDa experiments (Fig. 2.5a, b, c). Additionally the amount of dextran transported across the hfRPE cells, decreased with the increasing molecular weight of the FITC dextran encapsulated in the hydrogel-loaded microdevices (Fig. 2.5d). These results have led us to conclude that our planar microdevices can be used to successfully transport large molecules across different types of retinal epithelial cells. Of greater significance is the consistent performance of the device and its drug transport across these two *in vitro* RPE models. Further this suggests that these planar microdevices could be effective in transporting therapeutics in an *in vivo* model.

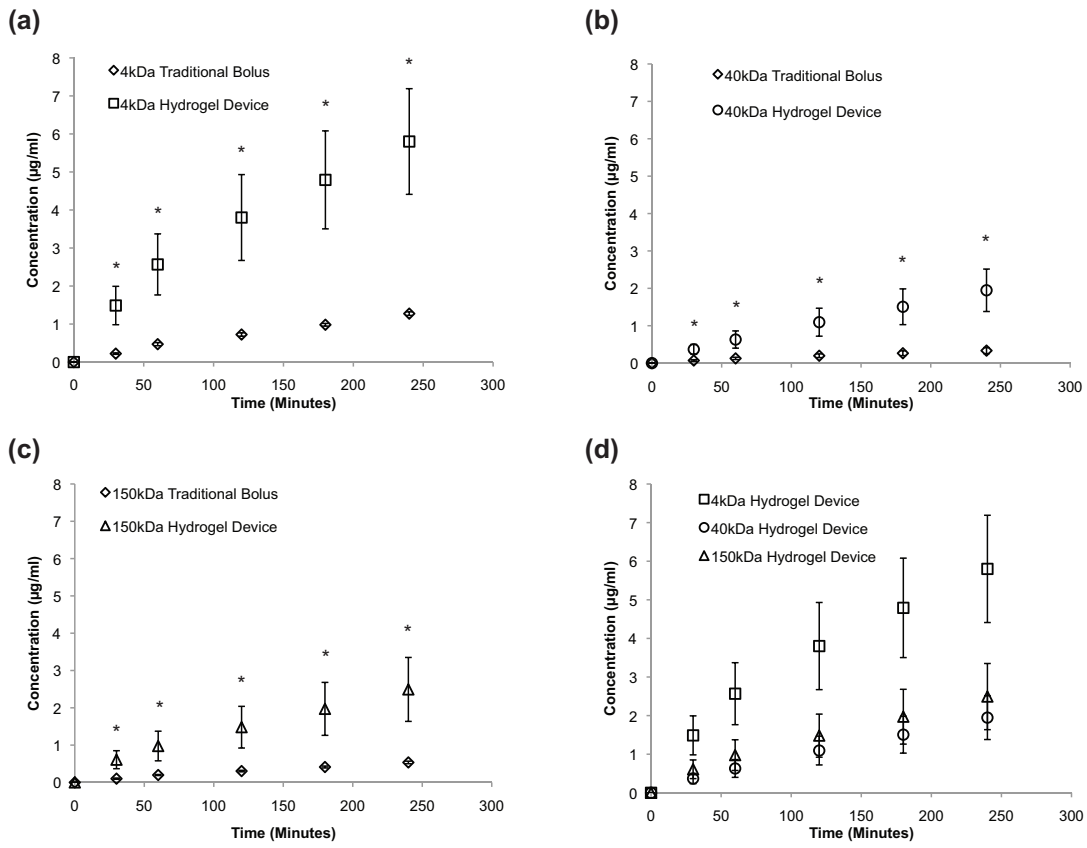

Figure 2.5 hfRPE Permeability Studies. Transport of FITC dextran across a monolayer of hfRPE cells grown on transwell inserts using a traditional bolus and planar hydrogel devices. FITC dextran of varying molecular weights (a) 4 kDa, (b) 40 kDa, (c) 150 kDa was deposited in the apical chamber and encapsulated in the uncoated planar SU-8/PEDGMA devices for each experiment. (d) The concentration of drug transported is molecular weight dependent. An asterisk (*) indicates statistical significance with respect to the traditional bolus conditions. All data is presented as +/- standard deviation.

To obtain additional insight into the mechanism of transport in the hfRPE experiments qPCR was conducted post drug transport experiment. Paracellular transport was considered a primary method of transport due to the large molecular weight of the FITC dextrans used in this study [62,88,89]. The cells were probed for expression of ZO-1 and Occludin, two tight junction proteins, which are responsible for restricting paracellular transport. It has been documented that reduced gene expression of tight junction proteins such as ZO-1 correlates with leaky tight junctions and increased permeability [39,90].

Expression of both ZO-1 and Occludin mRNA in the presence of the traditional bolus was significantly higher than all of the other delivery modes for the 40 kDa experiments (Fig. 2.6a). This was consistent with the 4 kDa dextran experiments and supports the observed reduced transport of FITC dextran when administered via traditional bolus as compared to microdevice delivery (Fig. 2.5a, b, c). The hydrogel-loaded microdevice and empty device both reduced ZO-1 and Occludin mRNA compared to untreated hfRPE cells. This observation led us to conclude that the devices helped facilitate transport of a 40 kDa molecule via a paracellular pathway by triggering the decreased production of two tight junction proteins. Since all microdevices are cleaned, prior to contact with the cells, it is unlikely that trace chemicals from the fabrication process caused a reduction in gene expression. It is probable that direct contact between the topography of the planar device and the cell membrane initiated a signaling mechanism, which reduced tight junction gene expression [46,91,92].

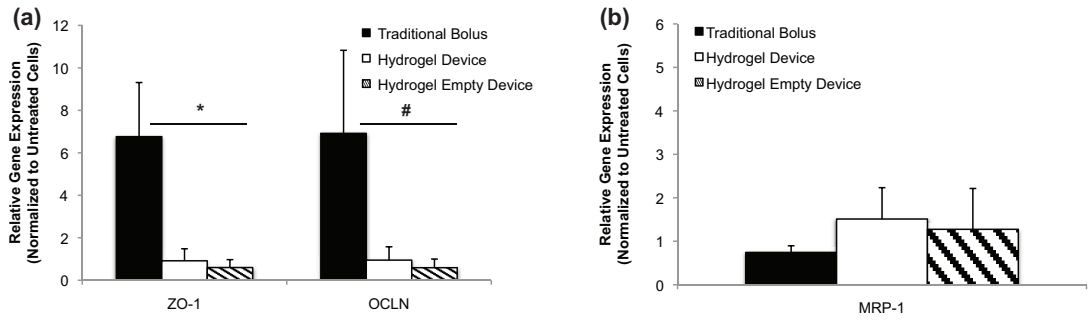

Figure 2.6 Quantitative PCR Studies (hfRPE). Relative gene expression of (a) tight junction proteins post planar microdevice permeability study [40 kDa FITC dextran]. (b) Relative gene expression of MRP-1 efflux transporter protein post planar microdevice permeability study [40 kDa FITC dextran]. All data is normalized by the gene expression of the control (untreated cells) and presented as mean +/- standard deviation. An asterisk (*) indicates statistical significance with respect to the traditional bolus of less than 0.05 and a hash mark (#) indicates statistical significance with respect to the traditional bolus of less than 0.07.

Based on the possibility that a mechanism other than paracellular transport could be involved, the cells were also probed for gene expression of the efflux transporter multidrug resistance protein (MRP-1). MRP-1 has broad substrate specificity and is highly expressed in retinal cells [25,61,93–95]. The traditional bolus showed a slightly decreased expression of MRP-1 mRNA as compared to the hydrogel-loaded and empty microdevices (Fig. 2.6b). There was however, no statistically significant difference in MRP-1 expression between the three routes of drug delivery. This suggests that MRP-1 does not play a major role in the facilitation nor hindrance of the FITC dextran transport. Combined with the ZO-1 and Occludin data, this suggests that the paracellular pathway plays a major role in the transport of FITC dextran to the basolateral chamber. This is consistent with what was expected given the size of the molecules, despite the substrate specificity of FITC to the MRP-1 efflux transporter. Building on these data, future work will target a broader set of efflux and influx transporters to understand the role they play in large molecule drug transport in the presence of planar microdevices.

2.4 Conclusion

A planar microdevice has successfully transported large molecules, with molecular weights of therapeutic significance, across both ARPE-19 and hfRPE cells *in vitro*. The microdevices increased the delivery of FITC dextran across an ARPE-19 and hfRPE barrier as compared to bolus administration in a molecular weight dependent fashion. This was achieved through a device triggered paracellular pathway while maintaining the

integrity of the retinal cell monolayers. Further studies to understand the dominant paracellular mechanism and corresponding signaling cascade are necessary.

Chapter 3: Surface-Modified Planar Microdevices for Large Molecule Transport Across Retinal Pigment Epithelial Cells

3.1 Background

Prior to the use of microfabricated devices to improve drug delivery, permeation enhancers were studied extensively. The most commonly investigated formulations include Tween20, ethylenediaminetetra acetic acid (EDTA), dimethylsulphoxide (DMSO) and cyclodextrin. Their use has been found to increase the bioavailability of a diverse set of small molecules in ocular applications [96–98]. However, these compounds were regularly implicated in causing irreversible damage to cell barrier integrity [66]. Additionally, due to the importance of therapeutic residence time for increased bioavailability, mucoadhesive formulations for drug delivery have been explored [99,100].

An alternative to these compounds is Chitosan, a polysaccharide with demonstrated permeation enhancing properties in epithelial cell lines [58]. Chitosan is a naturally occurring polymer that is derived from the deacetylation of chitin found in the shells of crustaceans [101,102]. It is regularly considered for use in drug delivery applications due to several attractive features. These features include biocompatibility, mucoadhesive properties, known enzymatic degradation pathways and its ease of acquisition [103–106]. Further chitosan is highly stable and can be incorporated into delivery systems in a variety of formulations such as particles, hydrogels, liquid gels and films [52,103,107–109]. De Campos et al demonstrated a 10-fold increase in transport of cyclosporine-A

using chitosan nanoparticles in an *in vivo* rabbit experiment [110]. Prednisolone bioavailability was also enhanced using self-assembled chitosan nanoparticles [111]. Small molecules have historically been the therapeutic of choice for delivery using chitosan. Recently, several groups have investigated macromolecule delivery of vaccines and dextrans using chitosan formulated microparticles [56,112].

Chitosan is able to enhance permeability due to the interaction of its cationic amino acid groups with the negatively charged membrane of epithelial cells [58,113,114]. It is believed that this leads to a relocation of the epithelial tight junction proteins ZO-1 and occludin, thus permitting increased paracellular transport [56,57,105,115]. Chitosan's mucoadhesive properties are primarily caused by an electrostatic attraction [57,105,116].

Building upon our success in transporting large molecular weight dextrans with planar microdevices (Chapter 2) we incorporated chitosan to investigate a dual permeation enhancing effect. The subsequent experiments investigate the transport of a commercially available therapeutic (Lucentis®) using a chitosan planar device. We also explore the impact of chitosan devices in the transport of three distinct molecular weight FITC Dextrans.

3.2 Materials & Methods

3.2.1 Materials:

ARPE-19 cells were obtained from American Type Culture Collection (ATCC). Dulbecco's modified eagle medium (DMEM:F12 [1:1]) for cell culture, Fetal Bovine

Serum, Penicillin-streptomycin antibiotic solution, PBS and mouse laminin were obtained from the UCSF Cell Culture Facility. Ranibizumab (Lucentis®) was manufactured by Genentech (South San Francisco, CA). Transwell inserts, Chitosan and FITC dextran spanning molecular weights of 4 to 150 kDa were obtained from Sigma-Aldrich. The EZ-Link Sulfo-NHS-LC-Biotin and corresponding FITC-avidin were purchased from Thermo Fisher Scientific. FluoroTag FITC conjugation kit for antibodies was purchased from Sigma-Aldrich. The hydrogel precursor solution, comprised of PEGDMA (750 mol. wt.), dimethoxy-phenyl acetophenone (DMPA) and polyvinylpyrrolidone (PVP) was purchased from Sigma-Aldrich. The SU-8 photoresist was purchased from Microchem (Newton, MA).

3.2.2 Cell Culture:

The ARPE-19 cell line was derived from the normal eyes of a 19 year-old male. The cells were grown in a T-75 flask with a 1:1 mixture of DMEM:F12 high glucose media containing 10% Fetal Bovine Serum (FBS) and 1% Penicillin-streptomycin antibiotic solution. The *in vitro* retinal model was constructed using a 24-well, high density 0.4μm transwell filter insert and plate assembly. The transwell filter inserts were coated with a 1:10 mouse laminin-DMEM:F12 serum free mixture and allowed to dry overnight in a cell culture hood. The ARPE-19 cells were seeded on the filters at a density of 4.5×10^5 per insert. The media used for the transwell inserts, is the same as described above with the exception of the fetal bovine serum, which is added at 1% of the total volume. All cells were maintained at 37°C in 5% CO_2. ARPE-19 cells were used between passages 25 and 35.

3.2.3 Device Fabrication & Surface Modification:

The body of the microdevice was fabricated from SU-8 and a PEGDMA hydrogel using photolithography as described in Chapter 2 (Section 2.2.3). After successful fabrication of a drug loaded hydrogel device chitosan was conjugated to the top surface of the planar device. A stock solution of chitosan was made by adding it to 1% HCl to obtain a 1.6 % w/v solution. This solution was mixed overnight using a stir bar and was mixed in this fashion prior to each use. In a separate falcon tube 1 mL of the chitosan-1% HCl stock solution was added to 3 mL of PBS and vortexed. Approximately 1 mL of the combined solution was deposited on top of the wafer until the devices were fully covered. The wafer was then allowed to dry overnight at 4°C. For visualization, 5 mg of EZ-Link Sulfo-NHS-LC-Biotin is added to the chitosan solution, vortexed and then deposited on the device covered wafer prior to drying as described above. The devices were then washed three times with PBS and blocked with 1% BSA for 30 minutes. A 1 mg/mL concentration of FITC-avidin was mixed with PBS at a 1:200 ratio. The devices were then incubated in this solution overnight. After incubation the device covered wafer was washed three times PBS prior to imaging.

3.2.4 FITC Conjugation:

Lucentis® at a concentration of 10 mg/ml was generously donated by Robert Bhisitkul M.D., Ph.D. of UCSF. Fluorescein isothiocyanate (FITC) was conjugated to the antibody fragment, Lucentis®, using the FluoroTag conjugation kit from Sigma. The conjugation was conducted in accordance with the protocol provided by Sigma. Breifly, Lucentis®

was transferred out of its native 10 mM histidine buffer via dialysis overnight into PBS. A sodium carbonate-bicarbonate buffer (0.1 M) was used to reconstitute 2 mg of FITC. This FITC solution (10:1) was added dropwise to the Lucentis solution under gentle stirring. The solution was protected from light and allowed to mix at room temperature for 2 hours. All unbound FITC was then separated from the FITC conjugated Lucentis using a Sephadex G-25M column into glass vials. Each elution sample was probed using UV spectroscopy at 280 and 495 nm. Samples with absorbance values greater than 0.4 at 280 nm were pooled into a single vial; all others were discarded.

3.2.5 Transport Studies:

ARPE-19 cells were grown to confluence on porous transwell filter inserts in a 24-well plate. Confluency was measured using transepithelial electrical resistance (TEER). All transport studies were conducted on cells grown for four to six weeks on transwell filter inserts. Equal concentrations (13 μg/mL) of the desired therapeutic (FITC Lucentis or 4, 40 and 150 kDa FITC dextran) were deposited in the apical chamber of the transwell filter in one of three forms: a standard bolus, an uncoated or a chitosan coated planar microdevice. Cells alone and empty planar microdevices were used as controls. At periodic time points the entire volume of the basolateral chamber was removed and replaced with fresh Phosphate Buffered Saline (PBS). The samples were then probed for the concentration of FITC dextran, transferred to the basolateral chamber, using a fluorimeter. Prior to commencement of the transport studies the inserts were washed two times in PBS and transferred to a new 24-well plate. The media was replaced with phenol red free DMEM: F12 to prevent interference with the fluorimeter measurements.

3.2.6 Analytical Techniques:

The confluency of the ARPE-19 cells was measured using the World Precision Instruments transepithelial electrical resistance (TEER) device. Measurements were taken weekly until confluence was reached at approximately four weeks. The concentration of FITC-conjugated agents released from the microdevice was measured with a Packard FluoroCount fluorimeter.

3.3 Results & Discussion

3.3.1 Chitosan was Successfully Conjugated to Planar SU-8/PEGDMA Microdevices:

An existing drug loaded SU-8/PEGDMA microdevice was coated with the mucoadhesive and permeation enhancing agent chitosan (Fig. 3.1a). The coating is evenly distributed along the top surface of the individual devices. Additionally, there are traces of chitosan between devices which is anticipated based on the deposition process (Fig. 3.1b). chitosan distribution on top of the reservoirs is uneven and sparse. It is plausible that a low affinity exists between chitosan and PEGDMA. However, this coating discrepancy should not undermine the drug absorption enhancement effect of chitosan.

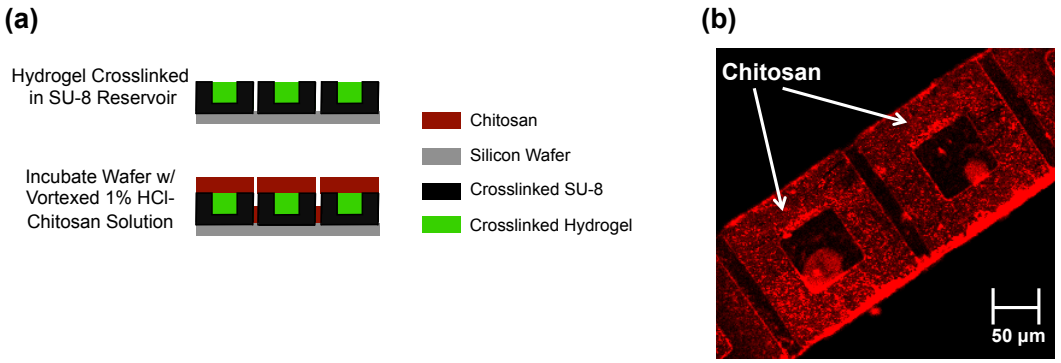

Figure 3.1 Chitosan SU-8/PEGDMA Device Fabrication Process. (a) Schematic representation of chitosan attachment to a SU-8/PEGDMA planar microdevice. (b) Image of FITC labeled chitosan affixed to the surface of an SU-8/PEGDMA device.

3.3.2 FITC Lucentis Transport is Not Enhanced By Chitosan Devices:

Transport of FITC Lucentis in the presence of a chitosan coated and uncoated device is comparable to bolus deposition alone (Fig. 3.2). As time progresses the amount of bolus FITC Lucentis transported begins to outperform both devices. Chitosan coating of the microdevice does not yield an improvement in drug transport irrespective of the permeation enhancing properties and unidirectional drug delivery design of the chitosan device. The chitosan device does begin to display a marginal improvement in drug transported relative to the uncoated device as the time course progresses. Surprisingly, the uncoated planar device does not enhance transport of FITC Lucentis relative to the traditional bolus. This is in stark contrast to the FITC Dextran transport trend observed in chapter 2 (Fig. 2.4 and 2.5). FITC Lucentis is a 48 kDa antibody fragment which we hypothesized would perform in a comparable fashion as the 40 kDa FITC Dextran. The 8 kDa increase in molecular weight should not justify the observed transport discrepancy as the 150 kDa FITC Dextran encapsulated in a hydrogel device also outperformed its respective traditional bolus.

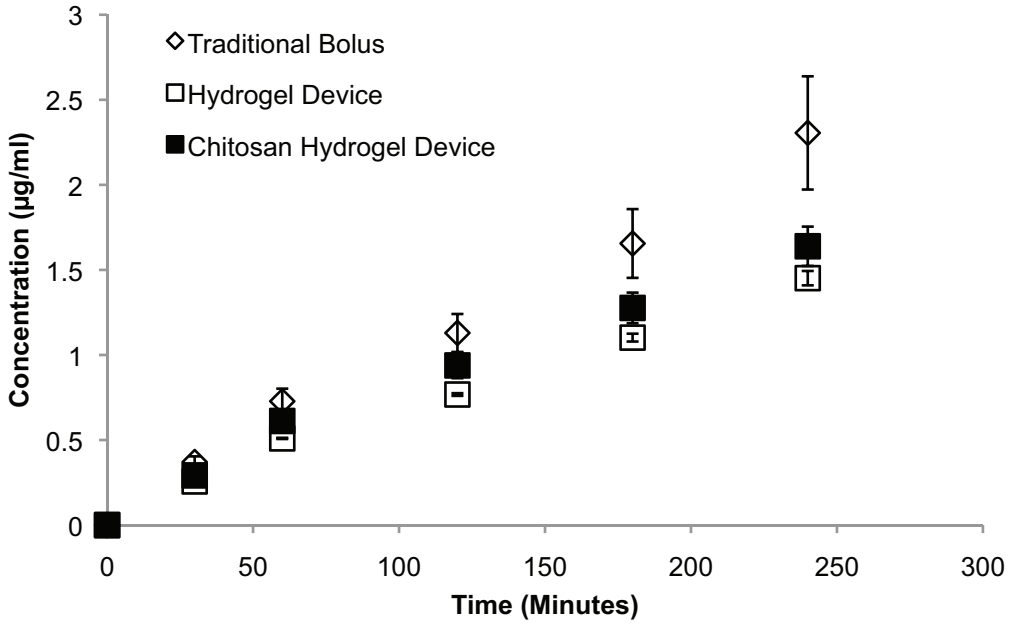

Figure 3.2 FITC Lucentis® Permeability Studies. Transport of FITC Lucentis® across a monolayer of ARPE-19 cells grown on transwell inserts using a traditional bolus, chitosan coated and uncoated planar SU-8/PEDGMA devices. All data is presented as +/- standard deviation.

3.3.3 FITC Dextran Transport is Not Enhanced by Chitosan Devices:

In figure 3.3 the transport of FITC Dextran encapsulated in a chitosan coated device is compared to an uncoated device. The uncoated device outperforms the chitosan device throughout the 4 and 40 kDa FITC Dextran experimental time course (Fig. 3.3a, b). It appears as if the presence of chitosan decreases the amount of drug transported. However, the difference in performance between the chitosan coated and uncoated device is negligible at 150 kDa (Fig. 3.3c). This is in stark contrast to a pronounced transport difference observed with the 40 kDa FITC Dextran coated and uncoated devices. This might suggest that the differences in transport seen with chitosan are negated at higher molecular weights due to size-dependent molecular interactions, which may retard elution from the hydrogel. It is also plausible that the method of chitosan incorporation

into the delivery device and chitosan concentration may play a critical a role in enhancing permeability [117]. The layer of chitosan increases the distance that an encapsulated drug must travel relative to the uncoated device. As a result the limited permeability observed could be due to an insufficient experimental time course. Further, the enhanced transport observed by De Campos et al in rabbit corneal epithelial cell lines occurred using nanoparticles that were fabricated primarily from Chitosan [110]. Additionally, the permeability phenomena observed by Dodane et al in Caco-2 cells was concentration dependent [55]. A planar device made entirely from chitosan might perform equivalently if not better than the SU-8/PEGDMA planar device.

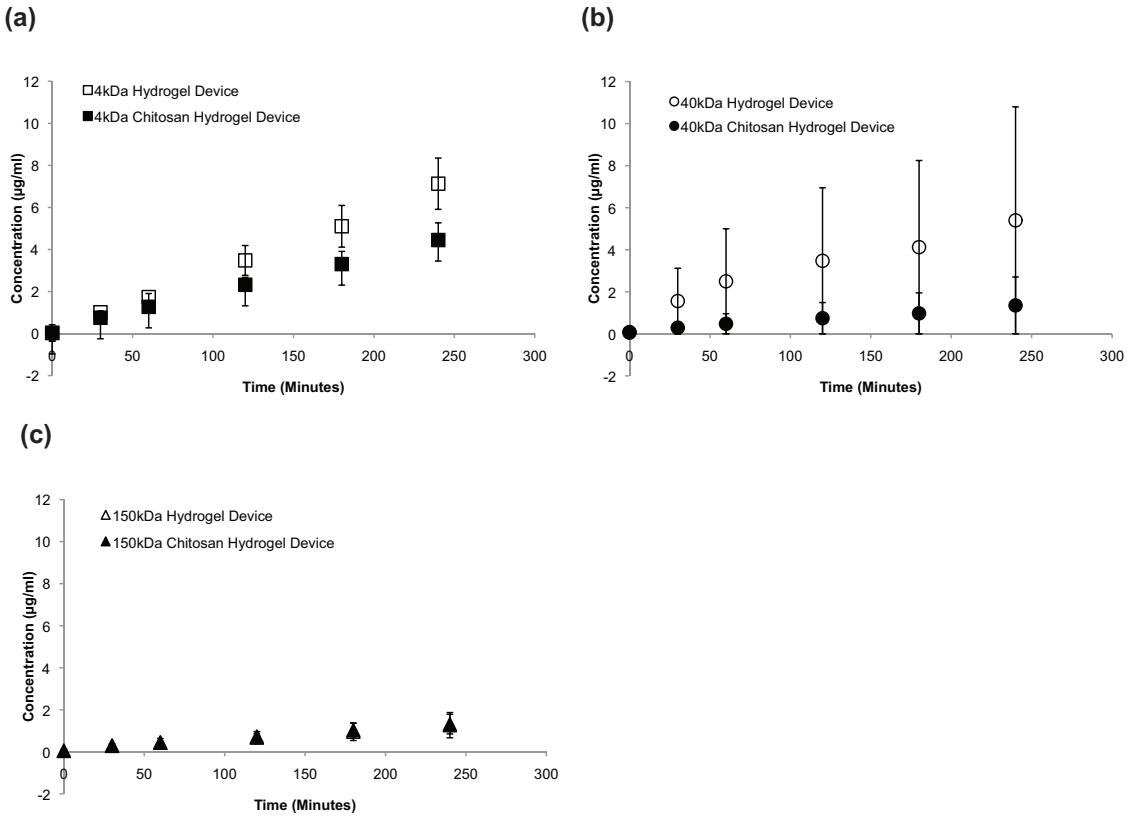

Figure 3.3 FITC Dextran Permeability Studies. Transport of FITC dextran across a monolayer of ARPE-19 cells grown on transwell inserts using chitosan coated and uncoated planar SU-8/PEDGMA devices. FITC dextran of varying molecular weights (a) 4 kDa, (b) 40 kDa, (c) 150 kDa was encapsulated in the uncoated planar SU-8/PEDGMA devices and deposited in the apical chamber for each experiment. The

concentration of drug transported is molecular weight dependent. All data is presented as +/- standard deviation.

3.4 Conclusion

Preliminary studies demonstrated the ability to conjugate chitosan to a drug loaded SU-8/PEGDMA planar microdevice. The chitosan devices did not enhance the transport of FITC conjugated large molecules, relative to uncoated devices, across a monolayer of ARPE-19 cells. Chitosan may still be a viable permeation enhancing agent to use in conjunction with a microdevice. However, an alternative fabrication process must be investigated to guarantee an equivalent drug elution profile relative to the device control. Additionally, the pH sensitivity of chitosan should be explored as this would help determine the ideal location for drug delivery.

Chapter 4: Micro- and Nanostructures for Macromolecule Transport Across Retinal Pigment Epithelial Cells

4.1 Background

Ocular diseases adversely impact the quality of life for 14.25 million people worldwide. Many of these impairments can be treated with commercially available therapeutics including 48 kDa antibody fragment Ranibizumab (Lucentis) [1,2]. Lucentis, is a widely used treatment for Wet Age-related Macular Degeneration (AMD). However, retinal epithelial barriers complicate delivery of such macromolecules to the treatment site [11,12,93]. Specifically, ZO-1 and Claudin tight junction proteins inhibit the paracellular transport of macromolecules [39,90,118]. To circumvent these barriers, many techniques have been explored to enhance ocular drug delivery. They include but are not limited to the use of permeation enhancers, surface conjugation strategies, viral infection, macroscale reservoir systems, and micro- and nanoscale devices [52,55,66]. While, the distinctions between macroscale and sub-macroscale devices are relatively straightforward, distinctions between micro- and nanoscale efficacy has yet to be extensively explored. Several methods used to fabricate these sub-macro reservoir systems, also known as microdevices, leverage micro- and nanofabrication techniques that were developed in the microelectronics industry to create devices and structures with precise geometries [81,82,84]. Microdevices have been designed to deliver a broad class of molecules using a variety of release techniques. These include mechanical actuators and environmentally responsive systems [78,119–123]. The Desai lab demonstrated that planar microdevices increased small and large molecule transport in an intestinal and

ocular epithelial model [83,124]. These devices leveraged their increased residence time, large contact surface area and unidirectional controlled release to increase drug transport. Further, a cell signaling mechanism triggered by the planar device topography was implicated in increasing large molecule permeability via paracellular transport [124]. Many researchers have begun to examine the effects of nanoparticle morphology on cell behavior [125,126]. They discovered that a variety of particle properties influence cell differentiation, morphology, proliferation, internalization, adhesion and protein expression [127–129]. These properties include particle surface charge, size, shape and chemistry [125,126]. Zauner et al found that nanoparticles are efficiently internalized by a variety of cell lines including the Caco-2 epithelial cell line [130,131]. However, there is still some debate about the range of sub-micron sizes that illicit the greatest uptake efficiency [125]. Numerous researchers have determined, *in vitro,* that positively charged particles and polysaccharides have enhanced transfection and permeation efficiency due to interaction with negatively charged cell membrane surfaces [55,58,88,116]. Also of interest is the role shape plays on drug transport and cellular transfection on both the micro- and nanoscale. In addition to the well-studied spherical shaped particles, several researchers have found that varying the aspect ratios and axis/radius of curvatures of particles can have a significant influence on the rates of uptake via receptor mediated endocytosis [132–134]. Specifically, Gratton et al found that larger aspect ratio particles yielded increased uptake. Kam et al reported enhanced paracellular transport of large molecules, using low aspect ratio nanostructured films in an intestinal epithelial cell model [91]. Both micro- and nanodevices have advantages which are size specific. However, to date no study has been undertaken to determine which size scale causes the

greatest enhancement of large molecule drug transport across ocular tissue. With this in mind, we sought to examine the role of micro- or nanostructure features on ocular permeability. Such topography-enhanced permeability may lead to novel treatment modalities but further study is necessary to optimize topographic geometry with specific properties of macromolecules. Using an epithelial model of the outer blood retinal barrier, we determine if macromolecule transport is preferentially enhanced as fiber size-scale is decreased from micro- to nanometers. Additionally, the impact of macromolecule size and charge on transport efficacy is investigated.

4.2 Materials & Methods

4.2.1 Materials:

Human fetal retinal pigment epithelial cells (hfRPE) were kindly donated by the National Eye Institute laboratory of Sheldon Miller Ph.D. Fetal Bovine Serum (FBS) was obtained from Atlanta Biologicals (Flowery Branch, GA). All remaining media components and FITC dextran spanning molecular weights of 40 to 150 kDa were obtained from Sigma-Aldrich (St. Louis, MO). FluoroTag FITC conjugation kit for antibodies was purchased from Sigma-Aldrich. Polyethylene terephthalate transwell inserts were purchased from Fisher Scientific (Waltham, MA). Polypropylene x-ray film was purchased from Premier Lab Supply (Port St. Lucie, FL). Polytetrafluoroethylene (PTFE) was obtained from McMaster-Carr (Santa Fe Springs, CA). Polystyrene was purchased from Sigma-Aldrich (St. Louis, MO) and polycarbonate filters with pore sizes of 0.4, 0.8 and 12μm were purchased from Millipore (Billerica, MA). Zonula Ocludens-1 (ZO-1) rabbit polyclonal antibody and rabbit anti mouse Alexa Fluor 633 secondary antibody were purchased from Zymed Laboratories (San Francisco,

CA) and Invitrogen (Grand Island, NY) respectively. Fast SYBR Green kit was purchased from Life Technologies (Grand Island, NY). Human extracellular matrix was purchased from VWR (Visalia, CA). Ranibizumab (Lucentis®) was manufactured by Genentech (South San Francisco, CA).

4.2.2 Cell Culture:

Human fetal retinal pigment epithelial (hfRPE) primary cells were provided as a gift from the laboratory of Dr. Sheldon Miller at the National Eye Institute of the NIH. Passage 0 flasks were provided with retinal cells derived from the eyes of a 16-18 weeks of gestation fetal donor. Briefly, the cells were grown in MEM-α mixture of media containing 5% heat inactivated FBS, N1 supplement (1:100 mL/mL), glutamine-penicillin-streptomycin (1:100 mL/mL), nonessential amino acid solution (1:100 mL/mL), hydrocortisone (20 µg/L), taurine (250 mg/L) and triiodo-thyronin (0.013µg/L). High density 24-well, 0.4µm transwell filter inserts were coated with a human extracellular matrix from human placenta in serum free MEM-α media, UV cured for 2 hours and allowed to dry overnight. The hfRPE cells were seeded on the filters at a density of 40 x 10^4 cells-cm^{-2}. All cells were maintained at 37°C in 5% CO_2. The hfRPE cells were seeded onto the inserts at passage 1 and were grown to confluence over a 6-8 week period.

4.2.3 Device Fabrication:

Nano- and microfiber films were fabricated by laminating polypropylene films into microporous polycarbonate filter membranes in a hot roll laminator (Cheminstruments,

HL-100), as described previously (Fig. 4.1) [135,136]. Briefly, polystyrene, dissolved in toluene (10% w/v), was spin cast onto a PET backing layer mounted on glass. The polystyrene was used to cap a polycarbonate filter membrane, which was then overlaid on pre-pressed polypropylene x-ray film. All layers were pressed through the hot roll laminator at 20 psi and 210°C protected by a sheet of PTFE. Polycarbonate filter membrane pore size was used to control fiber diameter, resulting in three distinct fiber sizes. Polycarbonate and polystyrene was etched away in two serial washes in methylene chloride for 8 minutes each.

4.2.4 Scanning Electron Microscopy (SEM):

Samples of micro- and nanofiber films were coated with 10 nm of iridium before imaging in an Carl Zeiss Ultra 55 Field Emission Scanning Electron Microscope using an in-lens SE detector at a beam voltage of 2 kV and a working distance of approximately 6 mm. Polypropylene fiber diameter and length were measured using a series of characteristic SEM images and analyzed with the open source Fiji image processing software.

4.2.5 Drug Conjugation:

Lucentis (10 mg/mL) was generously donated by Robert Bhisitkul M.D., Ph.D. of UCSF. Fluorescein isothiocyanate (FITC) was conjugated to the antibody fragment, Lucentis, using the FluoroTag conjugation kit from Sigma. The conjugation was conducted in accordance with the protocol provided by Sigma. Breifly, Lucentis was transferred out of its native 10 mM histidine buffer via dialysis overnight into PBS. A sodium carbonate-bicarbonate buffer (0.1 M) was used to reconstitute 2 mg of FITC. This FITC solution

(10:1) was added dropwise to the Lucentis solution under gentle stirring. The solution was protected from light and allowed to mix at room temperature for 2 hours. All unbound FITC was then separated from the FITC conjugated Lucentis using a Sephadex G-25M column into glass vials. Each elution sample was probed using UV spectroscopy at 280 and 495 nanometers. Samples with absorbance values greater than 0.4 at 280 nm were pooled into a single vial; all others were discarded. Drug concentration of the FITC conjugated solutions were determined by using Beer Lamberts law and the published extinction coefficients of 1.8 cm mL/mg for Lucentis [137].

4.2.6 Transport Studies:

Human fetal retinal pigment epithelial (hfRPE) cells were used for all transport studies. hfRPE mimic the morphological and physiological characteristics that occur *in vivo*, and therefore these primary cells are the preferred *in vitro* model of the retinal epithelium for permeability studies [85,87]. hfRPE cells were grown to confluency on porous transwell filter inserts in a 24-well plate. Confluency was measured using a transepithelial electrical resistance (TEER) device (World Precision Instruments). All transport studies were conducted on cells grown for six to eight weeks on transwell filter inserts. Inserts were washed twice in PBS and transferred to a new 24-well plate prior to initiation of the transport studies. The media was replaced with phenol red free DMEM: F12 to prevent interference with the fluorimeter measurements. Equal molar concentrations of the desired therapeutics (FITC-Lucentis and FITC-Dextran) were deposited in the apical chamber of the transwell filter. After drug deposition one of the three types of fiber films were placed on top of the cells (12 μm - Supermicro, 0.8 μm - Micro, 0.4 μm - Nano).

Film cross-sections with a diameter of 3.5 mm were used for transport studies by placing the fibers directly in contact with the monolayer of epithelial cells (Fig. 4.S1). Flat polypropylene films, untreated cells, and cells treated with drug alone were used as controls, the latter mimicking the injection of a bolus in proximity to the epithelial layer. At each time point the entire volume of the basolateral chamber was removed and replaced with fresh PBS. The samples were then probed for the concentration of FITC conjugated drug transported to the basolateral chamber, using a fluorimeter (Packard FluoroCount).

4.2.7 Calculation of Apparent Permeability Coefficient:

Apparent permeability coefficient ($P_{app,}$ cm/second) is a commonly used method to characterize the diffusion of molecules across an *in vitro* tissue barrier [49]. The equation is as follows: $P_{app} = Flux/(SA_{rpe}C_o)$, where flux is the slope of the permeability curve for each molecule (mM/second), SA_{rpe} is the surface area of the RPE coated transwell insert (cm^2) and C_o is the initial concentration of FITC conjugated drug loaded in the apical chamber (mM/cm^3).

4.2.8 Immunofluorescence:

hfRPE cells, grown on transwell filter inserts, were stained for the tight junction protein zonula occludens-1 (ZO-1) immediately after and 24 hours post exposure to micro and nanoscale fiber films. The duration of cell exposure to fiber films was 250 minutes without the addition of a FITC conjugated macromolecule. Cells were fixed for 30 minutes in 4% formaldehyde-PBS solution at 4°C and rinsed three times in PBS. The

cells were then permeabilized and blocked overnight with a 1% BSA- 0.1% Triton X solution at 4°C. A ZO-1 rabbit polyclonal antibody (Invitrogen) was diluted 1:100 in blocking solution and incubated with the samples overnight at 4°C. After rinsing in PBS, the cells were incubated in the dark with an Alexa Fluor secondary antibody (Invitrogen), and diluted 1:100 in blocking solution for 1 hour at 4°C. The samples were then mounted for spinning disk confocal imaging.

4.2.9 qPCR for Membrane and Tight Junction Gene Expression:

Cell lysis was conducted within one hour post conclusion of the transport studies. Lysis, reverse transcription and qPCR were performed using the Applied Biosystems SYBR Green Cells-to-CT kit per the manufacturer's instructions. Gene expression results are representative of three biological replicates, each an average of three technical replicates. The expression of GAPDH (forward 5'CTCTCTGCTCCTCCTGTTCG-3', reverse 5'GCCCAATACGACCAAATCC-3'), Claudin-19 (forward 5'CTCAGCGTAGTTGGCATGAA-3', reverse 5'GAAGAACTCCTGGGTCACCA-3'), Caveolin-1 (forward 5'GCGACCCTAAACACCTCAAC-3', reverse 5'ATGCCGTCAAAACTGTGTGTC-3') and Clathrin (forward 5'GTTTGATCGCCATTCTAGCCT-3', reverse 5'CTCCCACCACACGATTTTGCT-3') was analyzed using the specified primer sequences. The results were normalized to GAPDH transcript levels in untreated cells using the ΔΔCt method [138].

4.2.10 Statistical Analysis:

Data are reported as average values plus or minus standard deviation. All data sets were analyzed with a single factor ANOVA test followed by the Student-Newman-Keuls test. P-values of less than 0.05 were considered statistically significant unless explicitly stated otherwise.

4.3 Results

4.3.1 Fabrication of Controlled Micro and Nanofiber Films:

Polypropylene micro and nano structured thin films were fabricated using a novel lamination and wet etching process as described in the methods and outlined in figure 4.1a. During the lamination process the polypropylene is melted and forms individual fiber-like structures by filling the void space created by the pores in the polycarbonate filter membranes. Methylene chloride was used to etch away the filter resulting in a polypropylene thin film with a structured surface (Fig. 4.1b). The thin film is comprised of a polystyrene backing and individual micro- or nanoscale fibers made of polypropylene (Fig. 4.1c). Thin films with polypropylene fibers were successfully fabricated with diameters in the micrometer and nanometer ranges (Fig. 4.2a, b, c*)*. Three distinct fibers were generated, with diameters and lengths of 12.45 ± 0.08 μm and 7.645 ± 0.34 μm (supermicro), 0.973 ± 0.01 μm and 6.5 ± 0.42 μm (micro), and 0.549 ± 0.0009 μm and 5 ± 0.03 μm (nano), respectively. These fiber geometries will be referred to as supermicro, micro, and nanofiber films for the remainder of the text (Fig. 4.2d).

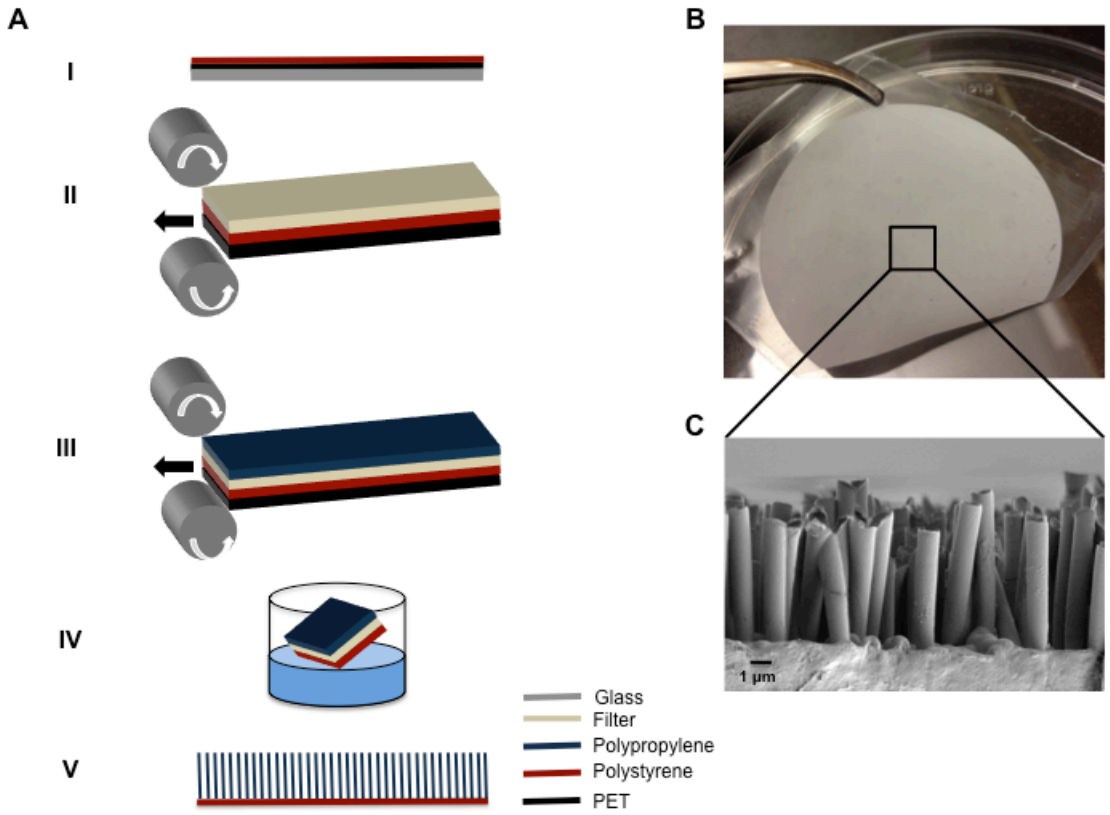

Figure 4.1 Polypropylene Micro and Nanofiber Thin Film Fabrication Process. (A) Schematic representation of fabrication using novel lamination and wet etching process to generate micro and nanoscale fibers. (B) Thin film post wet etching process (C) Scanning Electron Microscopy (SEM) image of a polypropylene thin film device with defined features.

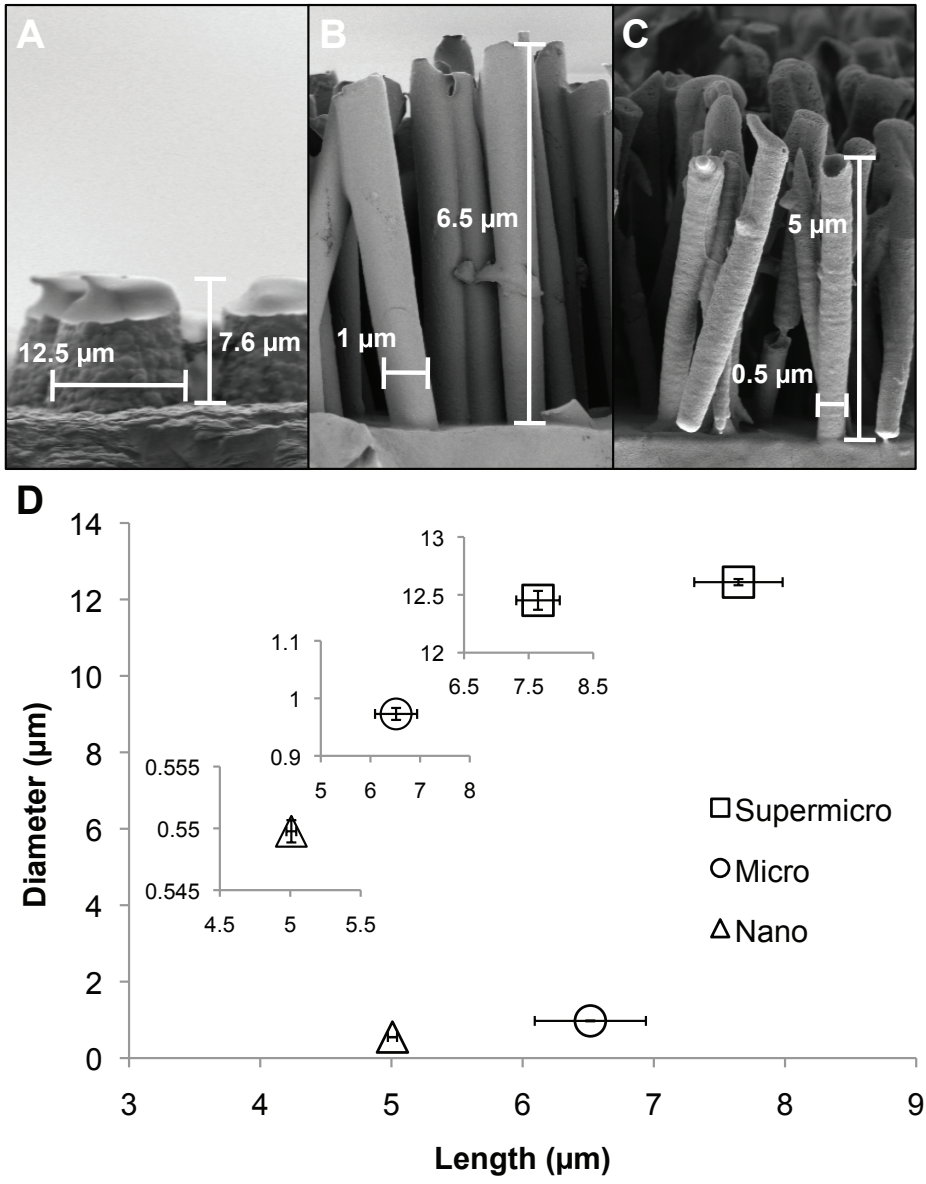

Figure 4.2 Scanning Electron Microscopy (SEM) of Structured Polypropylene Thin Films. (A) Polypropylene thin film with fibers formed from filters with pore diameters of 12 micrometers (B) 800 nanometers, and (C) 400 nanometers. (D) Characterization of average fiber length and diameter per thin film. All data is presented as +/- standard error.

4.3.2 Micro and Nanofibers Reversibly Disrupt hfRPE Tight Junction Morphology:

To investigate the effect of fiber morphology on paracellular transport in hfRPE, monolayers were stained for the tight junction protein Zonula Occludens 1 (ZO-1) after a 5-hour incubation with the fiber films. As seen in figure 4.3a, ZO-1 staining of an untreated monolayer is uniform and uninterrupted along the periphery of each cell. As the fiber dimensions decrease, ZO-1 staining becomes increasingly disrupted (Fig. 4.3b, c, d). Monolayers exposed to supermicrofiber films exhibit some remodeling of the ZO-1 protein localization in the form of sparsely distributed undulations (Fig. 4.3b). Treatment with microfiber films induces more pronounced undulations, along with sparse interruptions in ZO-1 staining along the cell periphery (Fig. 4.3c). However, monolayers treated with nanofiber films exhibit pronounced conformational changes, with numerous interruptions in ZO-1 peripheral staining and punctate staining mislocalized to the center of the cell body (Fig. 4.3d). Moreover, these dramatic conformational changes are reversible. Twenty-four hours after fiber film removal, ZO-1 staining in hfRPE monolayers reverts back to an uninterrupted configuration that resembles the untreated control (Fig. 4.3e, f, g).

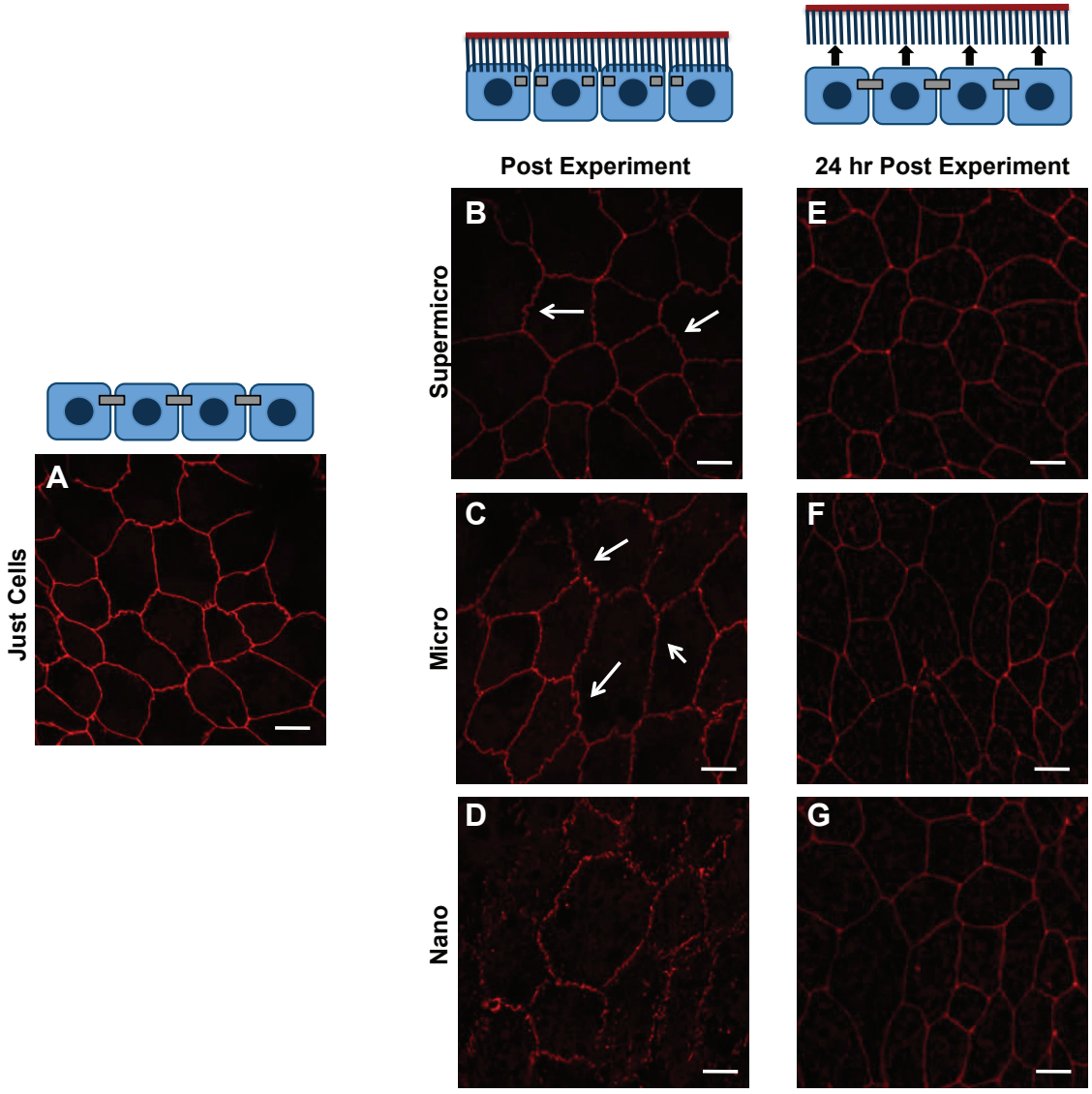

Figure 4.3 Conformational Tight Junction Disruptions. Immunofluorescence staining of the tight junction protein ZO-1 in (A) Untreated Cells, (B) cells in the presence of polypropylene Supermicro, (C) Micro and (D) Nanofiber thin films resulted in conformational changes. After 24 hours the tight junction conformation returns to a cobblestone morphology in the (E) Supermicro, (F) Micro and (G) Nano scenarios. These changes provide insight into the mechanism through which the nanofibers enhance Lucentis transport across human fetal retinal pigment epithelial cells.

4.3.3 Macromolecule Size and Charge alter Microfiber Film Transport Efficacy:

To determine the effect of fiber morphology on monolayer permeability, 40 kDa FITC dextran was added to the apical chamber of hfRPE monolayer cultures. There is a general trend of increased permeability in the presence of structured films as compared to bolus control (Fig. 4.4a). However transport of 40 kDa FITC Dextran, with and without structured films surpasses all other Dextran formulations (Fig. 4.4a, b). To determine if fiber film-induced permeability is dependent on molecular weight, monolayers were treated with 150 kDa FITC Dextran. The apparent permeability coefficient decreased for all treatments, including the bolus treated monolayer, as expected with an increase in molecular weight (Fig. 4.4a). Monolayers treated with both the micro and nanofiber films exhibited a dramatic decrease in transport of 150 kDa Dextran relative to 40 kDa Dextran, suggesting a size limitation for transport induced by fiber film treatment. To determine if fiber film-induced permeability is dependent on molecule charge, anionic and cationic 40 kDa FITC Dextrans were added to the apical chamber of hfRPE monolayers. Compared to neutral Dextran, the apparent permeability coefficient of charged 40 kDa Dextrans dropped for all treatments including the bolus-treated monolayers (Fig. 4.4b). However, the drop in permeability coefficients for anionic and cationic Dextrans differed for monolayers in contact with fiber films, indicating a charge preference in fiber film-induced permeability. Though permeability to cationic Dextran was decreased to approximately bolus levels for all fiber film treated monolayers, permeability to anionic Dextran was partially retained in monolayers treated with fiber films, nearly 70% for monolayers treated with supermicrofiber films (Fig. 4.4c).

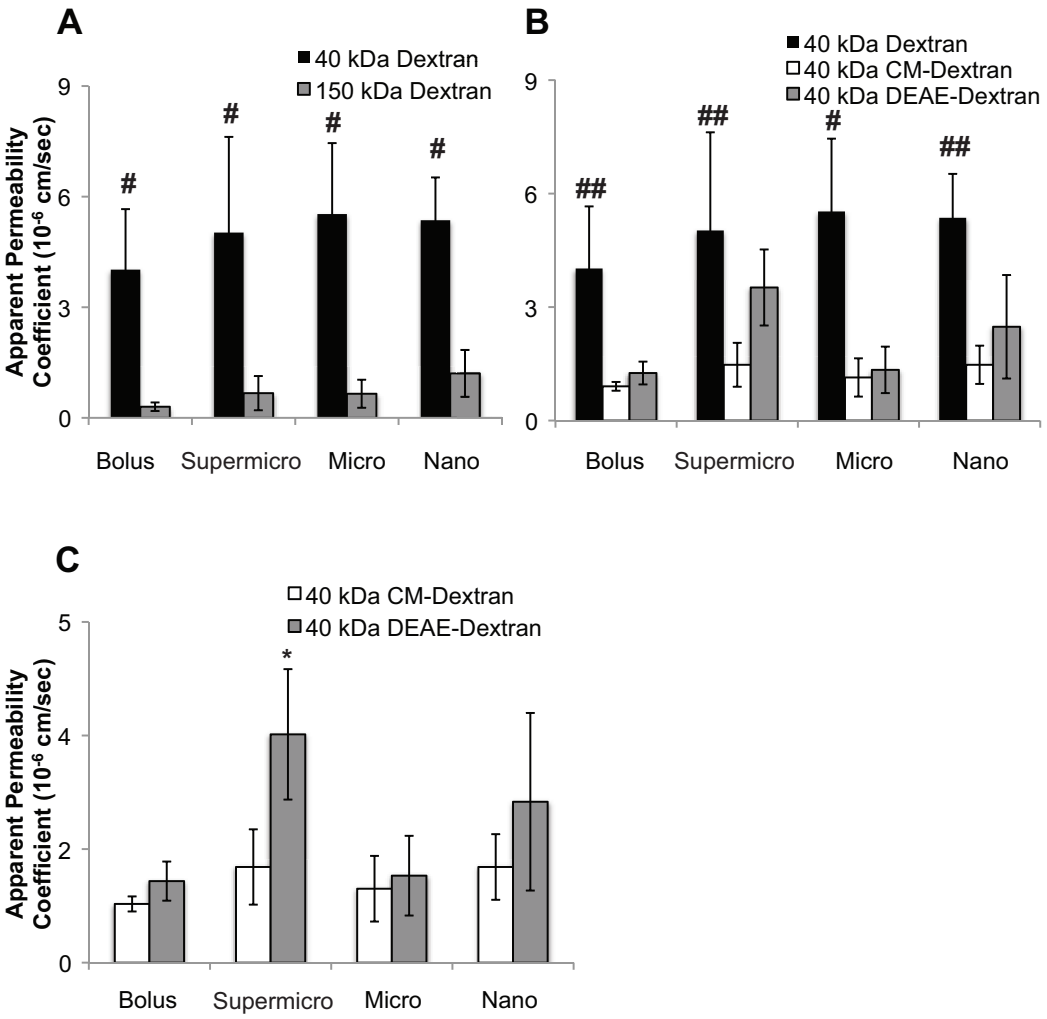

Figure 4.4 hfRPE Dextran Permeability Studies. Transport of FITC Dextran across a monolayer of human fetal retinal pigment epithelial cells grown on transwell inserts using a traditional bolus, polypropylene supermicro, micro and nanofiber films. Data presented as apical to basolateral apparent permeability coefficient. (A) Transport of neutral 40 kDa and 150 kDa FITC Dextran (B) Transport of anionic 40 kDa FITC DEAE-Dextran and cationic 40 kDa FITC CM-Dextran negates the transport advantage observed by the fiber films in the presence of neutral 40 kDa FITC Dextran. (C) Direct comparison of transport between cationic and anionic 40 kDa FITC Dextran highlights a charge dependent difference for supermicro and nanofibers. All data is presented as +/- standard deviation. An asterisk (*) indicates statistical significance of the supermicrofiber films with respect to the traditional bolus and micro conditions with a P-value of less than 0.03. A hash mark (#) indicates statistical significance between the respective device configurations of 40 kDa and 150 kDa neutral as well as 40kDa neutral, 40 kDa CM-Dextran and 40 kDa DEAE-Dextran with a P-value of less than 0.01. Two hash marks (##) indicates statistical significance between the respective device configurations of 40 kDa neutral and 40 kDa CM-Dextran with a P-value of less than 0.05.

4.3.4 Fibers Approaching the Nanoscale Enhance FITC Lucentis Transport Across Human Fetal Retinal Pigment Epithelium (hfRPE):

The data thus far indicate that uncharged macromolecules with a molecular weight close to 40 kDa are best suited for fiber film-induced transport across retinal pigment epithelium. Lucentis is a 48 kDa antibody fragment used to treat AMD, making it an ideal candidate for transport enhancement via fiber film application. To determine the effect of fiber films on epithelial permeability to Lucentis, hfRPE monolayers were treated with supermicro, micro, and nanofiber films in the presence of FITC Lucentis. The time course in figure 4.5a demonstrates that micro and nanofiber films induce a greater transport of Lucentis across hfRPE monolayers, outperforming both supermicro and bolus treated monolayer controls. We found that the apparent permeability coefficient of FITC Lucentis in the presence of micro and nanofiber films is 1.5 times greater than the either the supermicrofiber films or bolus treated controls (Fig. 4.5b).

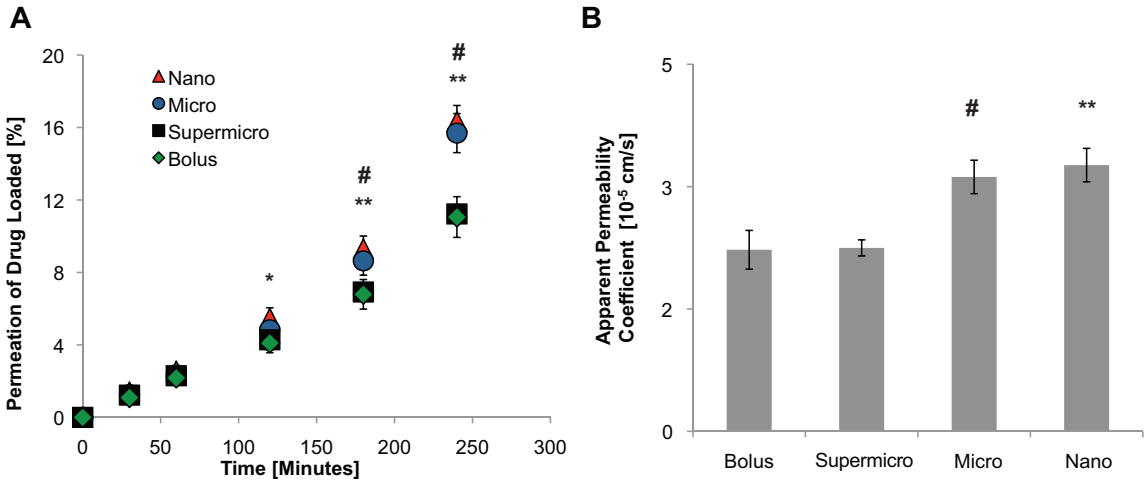

Figure 4.5 hfRPE Lucentis Permeability Studies. Transport of FITC Lucentis across a monolayer of human fetal retinal pigment epithelial cells grown on transwell inserts using a traditional bolus, polypropylene supermicro, micro and nanofiber films. (A) Transport of FITC Lucentis in the presence of the nanoscale fibers outperforms the supermicroscale fibers as time increases. (B) The apical to basolateral apparent permeability coefficient for the micro and nanofiber films surpass that of the

supermicro fiber films as well as the bolus control. All data is presented as +/- standard deviation. An asterisk (*) indicates statistical significance of the nanofiber films with respect to the traditional bolus and supermicro conditions with a P-value of less than 0.05. Two asterisks (**) indicate statistical significance of the nanofiber films with respect to the traditional bolus and supermicro conditions with a P-value of less than 0.01. A hash mark (#) indicates statistical significance of the microfiber films with respect to the traditional bolus and supermicro conditions with a P-value of less than 0.01.

4.3.5 Fibers Approaching the Nanoscale Reduce Tight Junction Specific Gene Expression:

To determine the effect of nano and microfiber films on transport in hfRPE monolayers gene expression of the transcellular transport genes Caveolin-1 and Clathrin, and the paracellular transport gene Claudin-19 was analyzed [41,133,139]. Compared to control cells that simulate a bolus injection *in vivo*, gene expression of Caveolin-1 and Clathrin was downregulated in the presence of all three fiber films (Fig. 4.6). However, there was no significant difference in gene expression of Caveolin-1 and Clathrin between the supermicro, micro, or nanofiber films, indicating that treatment with a fiber film downregulates transcellular transport genes irrespective of topography. However, expression of paracellular transport gene Claudin-19 was specifically knocked down by treatment with films containing fibers of micron and nanoscale diameters (Fig. 4.6). Treatment with supermicrofiber films had no effect, indicating that tight junction signaling may be sensitive to fiber dimensions.

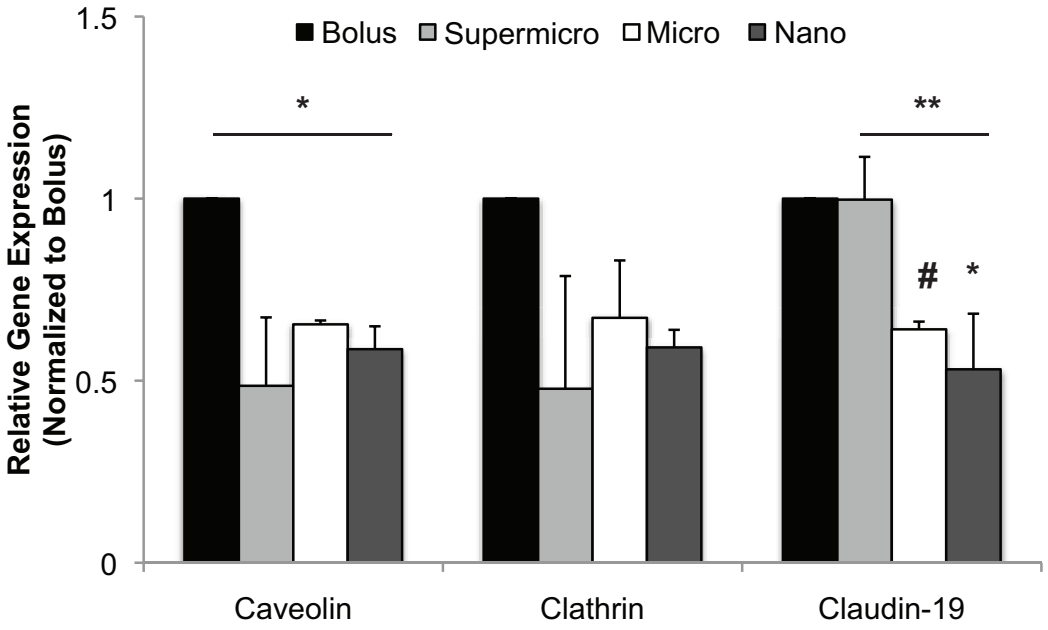

Figure 4.6 Quantitative PCR Studies (hfRPE). Relative gene expression of tight junction and transcellular transport proteins post FITC Lucentis permeability study in the presence of supermicro, micro and nano fiber polypropylene films. All data is normalized by the gene expression of the control (bolus treated cells) and presented as mean +/- standard deviation. An asterisk (*) indicates statistical significance with respect to the traditional bolus with a P-value of less than 0.01. Two asterisks (**) indicate statistical significance with respect to the supermicro fiber film with a P-value of less than 0.01. A hash mark (#) indicates statistical significance with respect to the traditional bolus with a P-value of less than 0.05.

4.4 Discussion

Understanding the role of varying topographies in the transport of large molecules is critical to optimizing the design of drug delivery devices. Micro and nanofiber polymer films are attractive because they are flexible, easily fabricated, can be tuned to various geometries and made from biocompatible or bioerodable materials (Fig. 4.1). In the present study, we aimed to understand what differences in macromolecular drug transport are mediated by micrometer versus nanometer size scales. To conduct this study it was essential that any fabrication variability between micro- and nanofiber films were minimized. The variability in diameter detected by SEM could be due to insufficient wet etching of the polycarbonate filter (Fig. 4.2d). However, the two-bath etching process

makes that an unlikely scenario. It is probable that variability in the filter pore size diameter contributes to these deviations. As the manufacturer acknowledges that effective diameter is closely controlled while the overall filter is highly tortuous with some pore irregularity. While duration of the lamination process is the main parameter for controlling fiber length, filter pore size is also a contributing factor. The observed variability in fiber length can be attributed to this.

It is well established that tight junctions restrict the movement of molecules between cells. Further, Koval et al report that tight junction protein ratios influence permeability in epithelial cells [43,140]. A tight junction protein of significance with respect to conferring barrier properties is ZO-1. In figure 4.3, the presence of micro- and nanofibers is clearly causing decreased expression as well as restructuring of the ZO-1 tight junction protein. This phenomena appears to increase with decreasing diameter and increasing aspect ratio of the polypropylene fibers (Fig. 4.3b, c, d). These data support the conclusion that paracellular transport is enhanced in the presence of these fiber films. Toxicity is a common phenomena with many permeation enhancement treatments [66,96]. As a result, the observed tight junction remodeling reversibility (Fig. 4.3e, f, g) is of great importance as it suggests this treatment modality would be non-toxic to cells.

It is established that transport behavior is influenced by the molecular weight, charge and shape of the drug [28,33]. Our experiments reinforced this known fact in the presence of the supermicro, micro- and nanofiber films (Fig. 4.4a, b, c). The behavior of neutral 40 kDa Dextran relative to its 150 kDa counterpart reinforced the known principle that

permeability decreases with increasing molecular weight. Unfortunately, increases in molecule size appear to eliminate the benefit conferred by the supermicro, micro- and nanofiber films (Fig. 4.4a). Anionic and cationic dextrans were used to understand the influence of charge. The overall concentration of dextran transported in the anionic experiment was greater with the aid of the supermicro fibers (Fig. 4.4c), which suggests that anionic molecules should be a target for drug delivery using topography based devices. Conversely, the permeability of cationic dextran in the presence of fiber films does not receive a significant enhancement, supporting the conclusion that a broad class of cationic molecules would not be ideal for delivery using this type of topography based device (Fig. 4.4c). Overall, when charge is involved marginal intrafiber film benefit can be identified in the cationic experimental conditions (Fig. 4.4c). While the permeability of anionic dextran is enhanced relative to cationic dextran, both charged dextrans display less permeability than neutral 40 kDa Dextran (Fig. 4.4b), suggesting that charge can hinder transport and further reinforcing the value of topographical cues to enhance drug permeability.

Our results indicate that micro- and nanofiber films are capable of enhancing the transport of FITC Lucentis, a 48 kDa commercially available antibody fragment (Fig. 4.5a). It is observed that nanofiber films enhance permeability as compared to supermicro fiber films and the existing standard of bolus administration (Fig. 4.5b). Further, the concentration of FITC Lucentis transported in the presence of micro- and nanofiber films exceeds that of neutral 40 kDa Dextran by a 5-fold magnitude. These data support the assertion that drug properties such as charge or structure influence

permeability irrespective of delivery device. It is plausible that a combination of transcellular and paracellular transport pathways were triggered by the polypropylene fibers [46]. The equivalent downregulation of transcellular markers Caveolin-1 and Clathrin could suggest that non-receptor mediated endocytosis does not provide the primary mechanism for the increased FITC Lucentis transport observed in the presence of the micro- and nanofibers (Fig. 4.6). An alternative conclusion is that the fibers could prohibit the use of some forms of endocytosis for FITC Lucentis transport. The authors did not investigate FcRn mediated endocytosis because it is unlikely to work in the transport of antibody fragments such as Lucentis [70,71]. Studies conducted by Peng et al have established the importance of Claudin-19 in conferring barrier properties to hfRPE cells [41,139]. Reduced expression of this tight junction protein in the presence of the micro- and nanofibers but not in the supermicro fiber film could have caused the enhanced paracellular transport (Fig. 4.6).

In summary micro- and nanofiber films with features that span a range of 500 to 1000 nanometers could be of greater value for the delivery of biologics than supermicro fiber films. These fiber films enhance transport of macromolecules across hfRPE cells through a paracellular pathway while maintaining cellular integrity. However, this advantage is negated by charge, aided by decreasing hydrodynamic radius and may be enhanced by molecule shape. This data provides insight for designing combination drug-device delivery systems. Further studies to understand the role of molecule shape and behavior of proteins with known endocytic pathways would be beneficial.

Chapter 5: Co-delivery with Efflux Pump Inhibitors Using Microdevices

5.1 Background

The previous chapters leveraged topography and surface chemistry to investigate the transport of macromolecules through paracellular pathways. Conversely, in this chapter we investigate small molecule transport through transcellular pathways. Small molecule absorption using membrane transporters for ocular drug delivery has recently become an area of focus for many researchers. It has been established that there are numerous transporters present in the apical and basolateral surfaces of the retinal pigment epithelium [141,142]. The presence of Multidrug Resistance-Associated Protein 1 (MRP-1), which is widely expressed in the body, is well known for its efflux pump properties. MRP-1 is a member of the ABC superfamily of transporters and typically confers multi-drug resistance to its host tissue. As such it will prevent a large range of drug substances from crossing the tissue membrane [94]. Previous studies have demonstrated that incubation of Caco-2 and Calu-1 cells with an efflux protein inhibitor, prior to administration of fluorescein or a therapeutic, will enhance the molecule accumulation in the cells [143]. Verapamil is a calcium channel blocker that is commonly used to inhibit the efflux properties of MRP-1 substrates through competitive inhibition [60,144]. Aukunuru et al demonstrated accumulation of N-[4-(benzoylamino)phenylsulfonyl] glycine (BAPSG) in both ARPE-19 and hfRPE cells when incubated with three known MRP-1 inhibitors, including verapamil [25]. Cole et al were also able to demonstrate increased transport of glutathione in the presence of verapamil [145]. Similarly, Ueda demonstrated the ability to limit transport of guanidine,

a known organic cation transporter (OCT) substrate, by inhibition through brimonidine incubation [146].

In many *in vitro* studies the inhibitor must be incubated with cells for a sufficient duration to elicit the desired permeation, enhancement or reduction, of the secondary drug target [147]. Some challenges with translating this combination therapy for ocular applications could be patient compliance with a two-step administration process and drug residence time. As a result, a microdevice that could co-administer an efflux inhibitor and a therapeutic would be valuable. Ainslie et al successfully demonstrated encapsulation of three macromolecules in a single reservoir of a planar microdevice [81]. Extending this work Chirra et al developed a planar microdevice with three distinct reservoirs, which were tuned to independently release their payloads at different rates [83].

Building upon established Desai laboratory fabrication techniques, we investigated the efficacy of efflux pump inhibition using two types of microfabricated small molecule co-delivery devices. The subsequent experiments investigate the transport of Fluorescein isothiocyanate (FITC) across retinal pigment epithelial cells using a multi-reservoir microdevice and a hydrogel cuboid.

5.2 Materials & Methods

5.2.1 Materials:

Human fetal retinal pigment epithelial cells (hfRPE) were kindly donated by the National Eye Institute laboratory of Sheldon Miller Ph.D. Fetal Bovine Serum (FBS) was obtained from Atlanta Biologicals (Flowery Branch, GA). All remaining media components, FITC, Verapamil and transwell inserts were obtained from Sigma-Aldrich (St. Louis, MO). The hydrogel precursor solution, comprised of PEGDMA (750 mol. wt.), dimethoxy-phenyl acetophenone (DMPA), polyvinylpyrrolidone (PVP) and monomer monomethyl methacrylate (MMA) was purchased from Sigma-Aldrich. The poly(methyl methacrylate) (PMMA) and Shipley 1818 positive photoresist was purchased from Microchem (Newton, MA).

5.2.2 Cell Culture:

Human fetal retinal pigment epithelial (hfRPE) primary cells were provided as a gift from the laboratory of Dr. Sheldon Miller at the National Eye Institute of the NIH. Passage 0 flasks were provided with retinal cells derived from the eyes of a 16-18 weeks of gestation fetal donor. Briefly, the cells were grown in MEM-α mixture of media containing 5% heat inactivated FBS, N1 supplement (1:100 mL/mL), glutamine-penicillin-streptomycin (1:100 mL/mL), nonessential amino acid solution (1:100 mL/mL), hydrocortisone (20 µg/L), taurine (250 mg/L) and triiodo-thyronin (0.013µg/L). High density 24-well, 0.4µm transwell filter inserts were coated with a human extracellular matrix from human placenta in serum free MEM-α media, UV cured for 2 hours and allowed to dry overnight. The hfRPE cells were seeded on the filters at a

density of 40 x 10^4 cells-cm^{-2}. All cells were maintained at 37°C in 5% CO_2. The hfRPE cells were seeded onto the inserts at passage 1 and were grown to confluence over a 6-8 week period.

5.2.3 Uptake Assay:

hfRPE cells were seeded in a 96-well UV transparent plate at a density of 5 x 10^4 cells/well. All cells were grown overnight and maintained at 37°C in 5% CO_2. Cells were washed three times in PBS before beginning the uptake assay. hfRPE cells were incubated at 37°C in 5% CO_2 for 15 minutes in a range of verapamil concentrations (50 µL of 10, 100, 165, 200, 300 µM) diluted in phenol red free media. Control wells were incubated in drug and phenol red free media for the same duration. Post inhibitor incubation 150 µL FITC (10 µM) was added to the verapamil treated and control wells. After incubating for an additional 20 minutes the verapamil and FITC were aspirated from the wells. All cells were washed three times in PBS and replaced with fresh phenol red free media. The cells were then analyzed for the concentration of internalized FITC, using a Packard FluoroCount fluorimeter.

5.2.4 Device Fabrication:

The hydrogel cuboid device was fabricated using a one-mask process. A hydrogel solution was spun onto a silicon wafer and a 150 x 150 µm cube was patterned via UV initiated crosslinking. Two hydrogel solutions were used. Solution one (slow release) was comprised of PEGDMA (750 mol. wt.; 2 mL) mixed with the photoinitiator dimethoxy-phenyl acetophenone (DMPA; 300 µL of 60 mg/mL) in monomer

monomethyl methacrylate (MMA). Finally, FITC (600 µL of 7 mg/mL) was mixed into the hydrogel solution. Solution two (fast release) was comprised of MMA (1 mL), PEGDMA (750 mol. wt.; 1 mL) mixed with the photoinitiator dimethoxy-phenyl acetophenone (DMPA; 300 µL of 60 mg/mL) in monomer monomethyl methacrylate (MMA). Verapamil (600 µL of 20 mM) was mixed into the hydrogel solution. Both hydrogel formulations were used in the hydrogel cuboid and multireservoir planar microdevices.

The body of the microdevice was fabricated as previously described by Chirra et al [83]. Briefly, a two-mask photolithography and reactive ion etching (RIE) process were used to create the planar device base and corresponding reservoirs in PMMA. After removal of residual photoresist with a developer the wafer was cleaned thrice with deionized water followed by an isopropanol rinse. The wafer was then blown dry with nitrogen and baked for 2 minutes at 95°C to remove all impurities prior to hydrogel loading. The aforementioned FITC and verapamil loaded hydrogels were spun onto the patterned wafers and separately crosslinked into each reservoir using a two-mask photolithography process.

5.2.5 Transport Studies:

Human fetal retinal pigment epithelial (hfRPE) cells were used for all transport studies. hfRPE cells were grown to confluency for six to eight weeks on porous transwell filter inserts in a 24-well plate. Confluency was measured using the World Precision Instruments transepithelial electrical resistance (TEER) device. Inserts were washed

twice in PBS and transferred to a new 24-well plate prior to initiation of the transport studies. The media was replaced with phenol red free DMEM: F12 to prevent interference with the fluorimeter measurements. Equal concentrations of FITC were deposited in the apical chamber of the transwell filter in one of four forms: FITC Hydrogel, Verapamil-FITC Hydrogel, FITC Microdevice and Verapamil-FITC Microdevice. Cells alone and a traditional bolus were used as controls. At each time point the entire volume of the basolateral chamber was removed and replaced with fresh Phosphate Buffered Saline (PBS). The samples were then probed for the concentration of FITC transferred to the basolateral chamber, using a Packard FluoroCount fluorimeter.

5.2.7 qPCR for MRP-1 Gene Expression:

Cell lysis was conducted within one hour post conclusion of the transport studies. Lysis, reverse transcription and qPCR were performed using the Applied Biosystems SYBR Green Cells-to-CT kit per the manufacturer's instructions. Gene expression results are representative of three biological replicates, each an average of three technical replicates. The expression of GAPDH (forward 5'CTCTCTGCTCCTCCTGTTCG-3', reverse 5'GCCCAATACGACCAAATCC-3') and MRP-1 (forward 5'CTGTTTTGTTTTCGGGTTCC-3', reverse 5'GATGGTGGACTGGATGAGGT-3'), was analyzed using the specified primer sequences. The results were normalized to GAPDH transcript levels in untreated cells using the ΔΔCt method [138].

5.2.9 Statistical Analysis:

Data are reported as average values plus or minus standard deviation. All data sets were analyzed with a single factor ANOVA test followed by the Student-Newman-Keuls test. P-values of less than 0.05 were considered statistically significant unless explicitly stated otherwise.

5.3 Results & Discussion

5.3.1 Cellular Uptake of FITC Increases in the Presence of Verapamil:

Human fetal retinal pigment epithelial cells demonstrate an increased accumulation of FITC when incubated with concentrations of verapamil greater than 165 μM (Fig. 5.1). This substantial accumulation exceeded 500 % of the control for 165, 200 and 300 μM concentrations of verapamil. Conversely, cellular uptake of FITC for the 10 and 100 μM verapamil conditions is equivalent to the inhibitor free controls which is consistent with existing literature [25]. Increasing the concentration of verapamil did not result in a linear increase of FITC accumulation (data not shown) suggesting that a range of inhibitor concentrations must be tested to guarantee efficacy of *in vitro* drug uptake. This preliminary data provided sufficient justification to investigate co-delivery of verapamil and FITC in a microfabricated device.

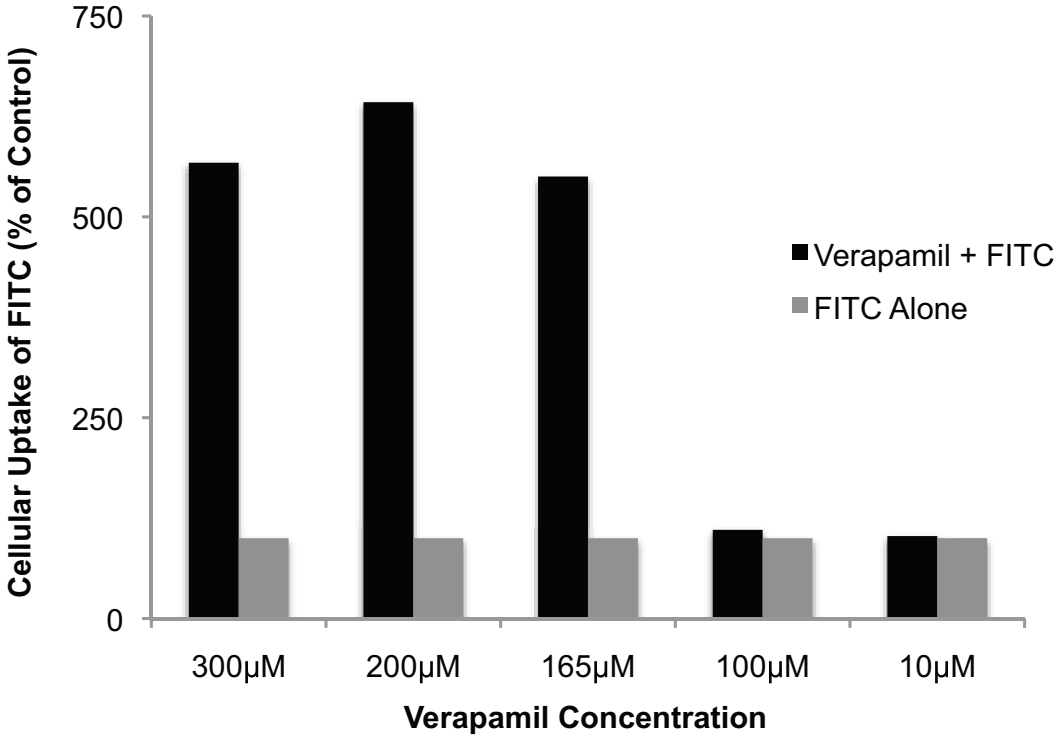

Figure 5.1 FITC Uptake Assay. Accumulation of FITC in human fetal retinal pigment epithelial cells when incubated with and without verapamil.

5.3.2 Device Characterization:

Hydrogel cuboid devices were fabricated with two distinct formulations to engender a burst release of verapamil and a controlled elution of FITC (Fig. 5.2a, b). Planar multireservoir microdevices were successfully fabricated using the protocol developed by Chirra et al [83]. Both FITC and verapamil were encapsulated in independent reservoirs using the aforementioned distinct hydrogel formulations (Fig. 5.2c, d).

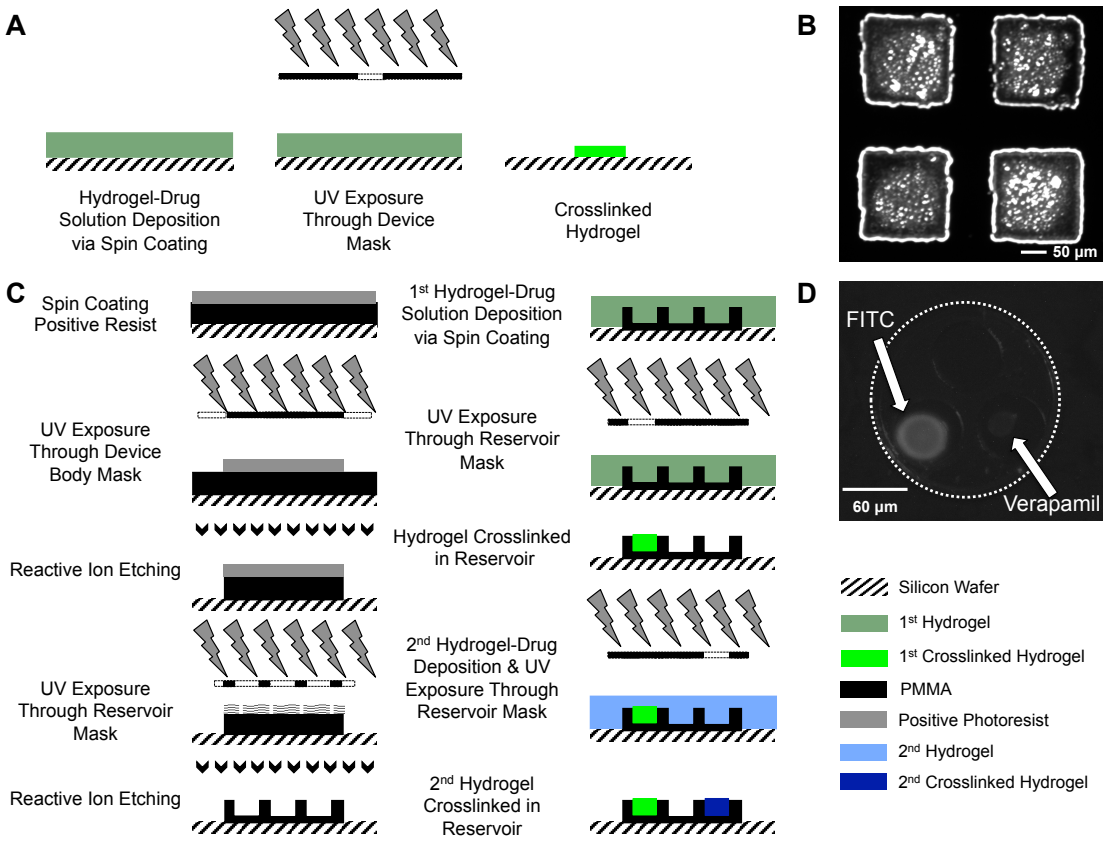

Figure 5.2 Microdevice Fabrication Process. (a) Schematic representation of hydrogel cuboid fabrication (b) Fluorescent microscopy image of hydrogel cuboid mounted on a silicon wafer (c) Schematic representation of multireservoir planar microdevice fabrication adapted from Chirra 2012 [83]. (D) Fluorescent microscopy image of FITC and verapamil encapsulated in independent reservoirs.

5.3.3 FITC Transport is Not Enhanced by Device Mediated Verapamil Co-delivery:

Transport of FITC encapsulated in hydrogel cuboid devices exceeds that of the verapamil and FITC co-administered hydrogel cuboids (Fig. 5.3a). This trend is consistent as the time course progresses suggesting that the co-delivery condition will not equalize with its respective FITC counterpart. FITC co-administered with verapamil in a multi-reservoir planar microdevice also fails to deliver a larger concentration of FITC than its inhibitor free counterpart (Fig. 5.3b). The independent FITC microdevice displays superior

transport performance starting at the first time point. Contrary to the trend observed in the uptake assay, verapamil does not enhance FITC permeability in the hydrogel cuboid nor microdevice experimental conditions. This discrepancy could be attributed to several scenarios. While hfRPE cells are grown to confluence in the 96-well plates, cell polarization does not occur prior to commencement of the uptake assay. As such localization of MRP-1 and other transporters, which are inhibited by verapamil, could vary after confluence and polarization is reached in the transwell inserts. Such a scenario could explain the disparity between the uptake assay and transport study. Further, while commonly used, verapamil specificity is not exclusive to MRP-1 as P-gp has also been implicated in its transport [30,148]. Hence, it is also plausible that verapamil successfully stimulated a membrane transporter to inhibit FITC permeability. Alternatively the traditional benefit of the verapamil could be negligible when compared to the transport enhancement properties of a planar microdevice.

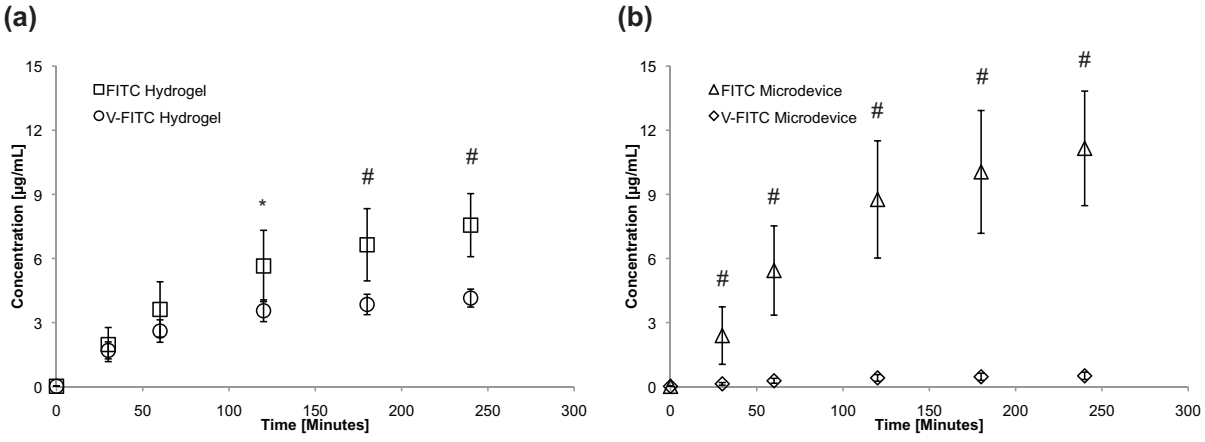

Figure 5.3 FITC Permeability Studies. Transport of FITC co-delivered with verapamil across a monolayer of hfRPE cells grown on transwell inserts using (a) hydrogel cuboid and (b) multireservoir planar microdevices. All data is presented as +/- standard deviation. An asterisk (*) indicates statistical significance with a P-value of less than 0.054. A hash mark (#) indicates statistical significance with a P-value of less than 0.02.

5.3.4 Co-delivery does not alter MRP-1 Gene Expression:

To determine if the negligible transport of FITC from the multireservoir microdevice is due to increased MRP-1 expression qPCR was conducted. hfRPE cells were treated with microdevices containing FITC, verapamil plus FITC, and corresponding bolus depositions of the same molecule combinations. No statistically significant difference in gene expression was observed between the verapamil loaded and unloaded microdevices (Fig. 5.4). Further, their MRP-1 gene expression was comparable to that of untreated hfRPE cells. Conversely, a traditional bolus of verapamil and FITC corresponded to an observed 50% increase in MRP-1 gene expression. Suggesting that verapamil can have an effect on polarized hfRPE cells however, it may be undetectable when delivered using a microdevice. It is probable that the difference in FITC transported is not due to MRP-1. The role of other transporters and tight junction proteins should be explored.

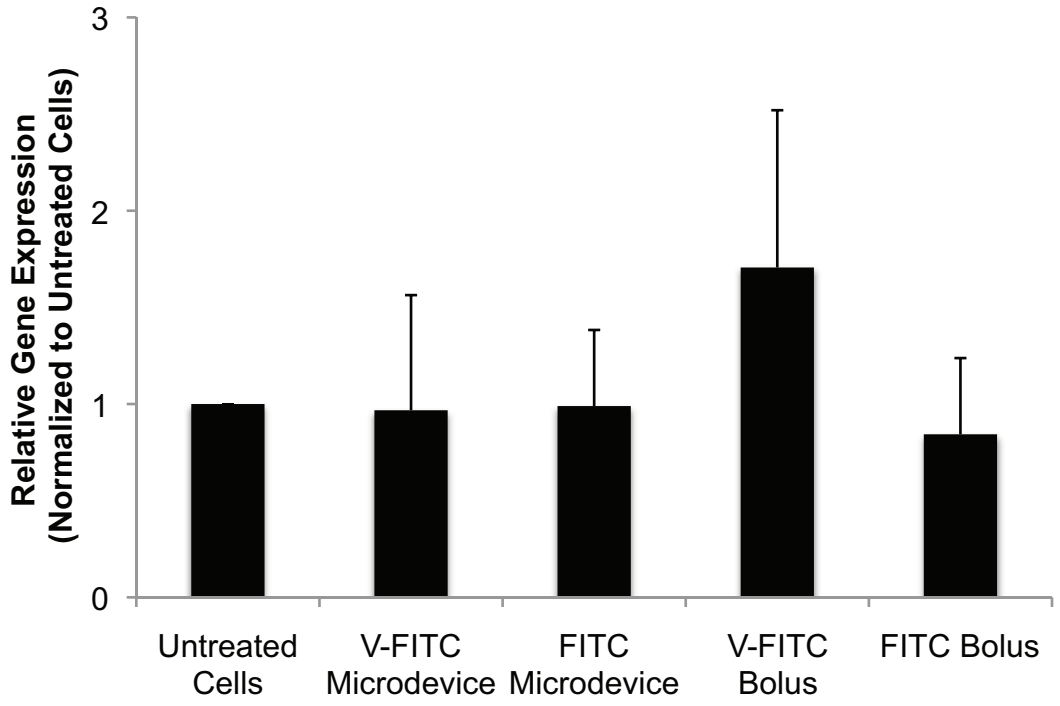

Figure 5.4 Quantitative PCR Studies (hfRPE). Relative gene expression of MRP-1 post FITC permeability study in the presence of multireservoir planar microdevices and traditional bolus depositions of FITC and verapamil. All data is normalized by the gene expression of the control (untreated cells) and presented as mean +/- standard deviation. An asterisk (*) indicates statistical significance with respect to the untreated cells with a P-value of less than 0.01. A hash mark (#) indicates statistical significance with respect to the untreated cells with a P-value of less than 0.05.

5.4 Conclusion

Two types of microdevices successfully transported FITC across hfRPE cells *in vitro*. The co-delivery of verapamil did not enhance FITC transport and may have limited its permeability across the RPE monolayer. Investigation into the localization of MRP-1, as well as other efflux transporters for which verapamil could be a substrate would help clarify this observation. Further, investigating co-delivery with two molecules that possess exclusive specificity for known transport modalities may provide a final evaluation on the suitability of multi-reservoir devices for this type of treatment.

References

1. Mariotti S. Vision 2020: The Right to Sight, The Global Initiative for the Elimination of Avoidable Blindness. World Health Organization, Geneva, Switzerland.

2. Mariotti S. Global Data on Visual Impairments 2010. World Health Organization, Geneva, Switzerland.

3. Friedman D. Prevalence of Age-Related Macular Degeneration in the United States. *Arch. Ophthalmol.* 122, 564–572 (2004).

4. De Jong PTVM. Age-Related Macular Degeneration. *N. Engl. J. Med.* 355, 1474–1485 (2006).

5. Ferrara N, Gerber H-P, LeCouter J. The Biology of VEGF and its Receptors. *Nat. Med.* 9(6), 669–676 (2003).

6. Ambati J, Ambati BK, Yoo SH, Ianchulev S, Adamis AP. Age-Related Macular Degeneration: Etiology, Pathogenesis, and Therapeutic Strategies. *Surv. Ophthalmol.* 48(3), 257–293 (2003).

7. Geroski DH. Transscleral Drug Delivery. In: *Drug Product Development for the Back of the Eye*. Edelhauser HF, Kompella UB (Eds.). Springer US, Boston, MA, 159–171 (2011).

8. Olsen TW, Gilger BC. Suprachoroidal and Intrascleral Drug Delivery. In: *Drug Product Development for the Back of the Eye*. Kompella UB, Edelhauser HF (Eds.). Springer US, Boston, MA, 173–184 (2011).

9. Tachikawa M, Ganapathy V, Hosoya K. Systemic Route for Retinal Drug Delivery: Role of the Blood-Retinal Barrier. In: *Drug Product Development for the Back of the Eye*. Kompella UB, Edelhauser HF (Eds.). Springer US, Boston, MA, 85–109 (2011).

10. Jager RD, Aiello LP, Patel SC, Cunningham ET. Risks of Intravitreous Injection: A Comprehensive Review. *Retina*. 24(5), 676–698 (2004).

11. Edelhauser HF, Rowe-Rendleman CL, Robinson MR, *et al.* Ophthalmic Drug Delivery Systems for the Treatment of Retinal Diseases: Basic Research to Clinical Applications. *Invest. Ophthalmol. Vis. Sci.* 51(11), 5403–5420 (2010).

12. Urtti A. Challenges and obstacles of ocular pharmacokinetics and drug delivery. *Adv. Drug Deliv. Rev.* 58(11), 1131–1135 (2006).

13. Hornof M, Toropainen E, Urtti A. Cell culture models of the ocular barriers. *Eur. J. Pharm. Biopharm.* 60(2), 207–225 (2005).

14. Barar J. Ocular Novel Drug Delivery: Impacts of Membranes and Barriers. *Expert Opin. Drug Deliv.* 5(5), 567–581 (2008).

15. Toropainen E. Corneal epithelial cell culture model for pharmaceutical studies. (2007).

16. Becker U. Examination of the penetration behavior of pharmaceutical drugs on the eye and set-up of an in vitro cell model for ocular drug delivery. (2006).

17. Prausnitz MR, Noonan JS. Permeability of Cornea, Sclera, and Conjunctiva: A Literature Analysis for Drug Delivery to the Eye. *J. Pharm. Sci.* 87(12), 1479–1488 (1998).

18. Mannermaa E, Vellonen K-S, Urtti A. Drug transport in corneal epithelium and blood–retina barrier: Emerging role of transporters in ocular pharmacokinetics. *Adv. Drug Deliv. Rev.* 58(11), 1136–1163 (2006).

19. Mannermaa E. In vitro Model of Retinal Pigment Epithelium for Use in Drug Delivery Studies. (2010).

20. Nickla DL, Wallman J. The Multifunctional Choroid. *Prog. Retin. Eye Res.* 29(2), 144–168 (2010).

21. Wilson CG, Zhu YP, Kurmala P, Rao LS, Dhillon B. Ophthalmic Drug Delivery. In: *Drug Delivery and Targeting For Pharmacists and Pharmaceutical Scientists*. Hillery AM, Lloyd AW, Swarbrick J (Eds.). Taylor and Francis, New York, NY, 329–354 (2001).

22. Kaur C, Foulds W, Ling E. Blood–retinal barrier in hypoxic ischaemic conditions: Basic concepts, clinical features and management. *Prog. Retin. Eye Res.* 27(6), 622–647 (2008).

23. Miller SS, Maminishkis A, Li R, Adijanto J. Retinal Pigment Epithelium: Cytokine Modulation of Epithelial Physiology. In: *Encyclopedia of the Eye*. Besharse J, Dana R, Dartt DA (Eds.). Academic Press, San Diego, CA, 89–100 (2010).

24. Olaf Strauss. The Retinal Pigment Epithelium in Visual Function. *Physiol. Rev.* 85, 845–881 (2005).

25. Aukunuru J, Kompella UB. Expression of Multidrug Resistance-Associated Protein (MRP) in Human Retinal Pigment Epithelial Cells and Its Interaction with BAPSG, a Novel Aldose Reductase Inhibitor. *Pharm. Res.* 18(5), 565–572 (2001).

26. Sunkara G, Ayalasomayajula SP, DeRuiter J, Kompella UB. Probenecid treatment enhances retinal and brain delivery of N-4-

benzoylaminophenylsulfonylglycine: An anionic aldose reductase inhibitor. *Brain Res. Bull.* 81(2-3), 327–332 (2010).

27. Mansoor S, Kuppermann BD, Kenney MC. Intraocular Sustained-Release Delivery Systems for Triamcinolone Acetonide. *Pharm. Res.* 26(4), 770–784 (2009).

28. Anya M. Hillery, Andrew W. Lloyd, James Swarbrick, editors. Drug Delivery: The Basic Concepts. In: *Drug Delivery and Targeting For Pharmacists and Pharmaceutical Scientists*. Taylor and Francis, New York, NY, 1–48.

29. Lee VHL, Yang JJ. Oral Drug Delivery. In: *Drug Delivery and Targeting For Pharmacists and Pharmaceutical Scientists*. Hillery AM, Lloyd AW, Swarbrick J (Eds.). Taylor and Francis, New York, NY, 145–183 (2001).

30. Han Y-H, Sweet DH, Hu D-N, Pritchard JB. Characterization of a novel cationic drug transporter in human retinal pigment epithelial cells. *J. Pharmacol. Exp. Ther.* 296(2), 450–457 (2001).

31. Mannermaa E, Vellonen K-S, Ryhänen T, *et al.* Efflux Protein Expression in Human Retinal Pigment Epithelium Cell Lines. *Pharm. Res.* 26(7), 1785–1791 (2009).

32. Daugherty AL, Mrsny RJ. Transcellular Uptake Mechanisms of the Intestinal Epithelial Barrier Part One. *Pharm. Sci. Technol. Today*. 2(4), 144–151 (1999).

33. Lin JH. Pharmacokinetics of Biotech Drugs: Peptides, Proteins and Monoclonal Antibodies. *Curr. Drug Metab.* 10, 661–691 (2009).

34. Kim H, Robinson SB, Csaky KG. FcRn receptor-mediated pharmacokinetics of therapeutic IgG in the eye. *Mol. Vis.* 15, 2803–2812 (2009).

35. Yuriko Ban, Atsuyoshi Dota, Leanne J. Cooper, *et al.* Tight junction-related protein expression and distribution in human corneal epithelium. *Exp. Eye Res.* 76, 663–669 (2003).

36. Daugherty AL, Mrsny RJ. Regulation of the intestinal epithelial paracellular barrier. *Pharm. Sci. Technol. Today*. 2(7), 281–287 (1999).

37. Rittenhouse KD. Drug Molecule Characteristics and Their Impact on Anterior Versus Posterior Segment Drug Delivery Strategies. In: *Ocular Drug Delivery Systems: Barriers and Application of Nanoparticulate Systems*. Thassu D, Chader GJ (Eds.). CRC Press, Boca Raton, FL, 285–300 (2013).

38. Juliano R, Bauman J, Kang H, Ming X. Biological Barriers to Therapy with Antisense and siRNA Oligonucleotides. *Mol. Pharm.* 6(3), 686–695 (2009).

39. González-Mariscal L, Nava P, Hernández S. Critical Role of Tight Junctions in Drug Delivery across Epithelial and Endothelial Cell Layers. *J. Membr. Biol.* 207(2), 55–68 (2005).

40. Cano-Cebrián MJ, Zornoza T, Granero L, Polache A. Intestinal Absorption Enhancement Via the Paracellular Route by Fatty Acids, Chitosans and Others: A Target for Drug Delivery. *Curr. Drug Deliv.* 2, 9–22 (2005).

41. Rizzolo LJ, Peng S, Luo Y, Xiao W. Integration of tight junctions and claudins with the barrier functions of the retinal pigment epithelium. *Prog. Retin. Eye Res.* 30, 296–323 (2011).

42. Tsukita S, Furuse M. Claudin-based barrier in simple and stratified cellular sheets. *Curr. Opin. Cell Biol.* 14, 531–536 (2002).

43. Koval M. Tight junctions, but not too tight: fine control of lung permeability by claudins. *Am. J. Physiol. Lung Cell. Mol. Physiol.* 297(2), L217–L218 (2009).

44. Peng S, Adelman RA, Rizzolo LJ. Minimal Effects of VEGF and Anti-VEGF Drugs on the Permeability or Selectivity of RPE Tight Junctions. *Invest. Ophthalmol. Vis. Sci.* 51(6), 3216–3225 (2010).

45. Salama NN, Eddington ND, Fassano A. Tight Junction Modulation and its Relationship to Drug Delivery. *Adv. Drug Deliv. Rev.* 58, 15–28 (2006).

46. Gonzalez-Mariscal L, Tapia R, Chamorro D. Crosstalk of Tight Junction Components with Signaling Pathways. *Biochim. Biophys. Acta*. 1778(3), 729–756 (2008).

47. Hillery AM, Lloyd AW, Swarbrick J, editors. Drug Delivery and Targeting For Pharmacists and Pharmaceutical Scientists. Taylor & Francis, New York.

48. Hosoya K, Yamamoto A, Akanuma S, Tachikawa M. Lipophilicity and Transporter Influence on Blood-Retinal Barrier Permeability: A Comparison with Blood-Brain Barrier Permeability. *Pharm. Res.* 27, 2715–2724 (2010).

49. Urtti A. Permeability of Retinal Pigment Epithelium Effects on Permeant Molecular Weight and Lipophilicity. *Invest. Ophthalmol. Vis. Sci.* 46(2), 641–646 (2005).

50. Choonara Y. A Review of Implantable Intravitreal Drug Delivery Technologies for Treatment of Posterior Segment Eye Diseases. *J. Pharm. Sci.* 99(5), 2219–2239 (2010).

51. Hamidi M, Azadi A, Rafiei P. Hydrogel nanoparticles in drug delivery. *Adv. Drug Deliv. Rev.* 60(15), 1638–1649 (2008).

52. Paolicelli P. Chitosan Nanoparticles for Drug Delivery to the Eye. *Expert Opin. Drug Deliv.* 6(3), 239–253 (2009).

53. Hiremath JG, Devi VK. Preparation and in vitro characterization of paclitaxel-loaded injectable microspheres. *Asian J. Pharm.* 4, 205–211 (2010).

54. Booth BA, Denham LV, Bouhanik S, Jacob JT, Hill JM. Sustained-Release Ophthalmic Drug Delivery Systems for Treatment of Macular Disorders Present and Future Applications. *Drug Aging*. 24(7), 581–602 (2007).

55. Dodane V. Effect of Chitosan on Epithelial Permeability and Structure. *Int. J. Pharm.* 182, 21–32 (1999).

56. Vllasaliu D, Exposito-Harris R, Heras A, *et al.* Tight Junction Modulation by Chitosan Nanoparticles: Comparison with Chitosan Solution. *Int. J. Pharm.* 400, 183–193 (2010).

57. Dornish M. Effect of Chitosan on Epithelial Cell Tight Junctions. *Pharm. Res.* 21(1), 43–49 (2004).

58. Schipper NGM, Varum KM, Artursson P. Chitosans as Absorption Enhancers for Poorly Absorbable Drugs. 1: Influence of Molecular Weight and Degree of Acetylation on Drug Transport Across Human Intestinal Epithelial (Caco-2) Cells. *Pharm. Res.* 13(11), 1686–1692 (1996).

59. Haghjou N, Abdekhodaie MJ, Cheng Y-L. Retina-Choroid-Sclera Permeability for Ophthalmic Drugs in the Vitreous to Blood Direction: Quantitative Assessment. *Pharm. Res.* 30(1), 41–59 (2012).

60. Toda R, Kawazu K, Oyabu M, Miyazaki T, Kiuchi Y. Comparison of drug permeabilities across the blood-retinal barrier, blood-aqueous humor barrier, and blood-brain barrier. *J. Pharm. Sci.* 100(9), 3904–3911 (2011).

61. Mannermaa E, Vellonen K-S, Urtti A. Drug transport in corneal epithelium and blood–retina barrier: Emerging role of transporters in ocular pharmacokinetics. *Adv. Drug Deliv. Rev.* 58(11), 1136–1163 (2006).

62. Kadam RS, Williams J, Tyagi P, Edelhauser HF, Kompella UB. Suprachoroidal delivery in a rabbit ex vivo eye model: influence of drug properties, regional differences in delivery, and comparison with intravitreal and intracameral routes. *Mol. Vis.* 19, 1198–1210 (2013).

63. Nirmal J, Sirohiwal A, Singh SB, *et al.* Role of organic cation transporters in the ocular disposition of its intravenously injected substrate in rabbits: Implications for ocular drug therapy. *Exp. Eye Res.* 116, 27–35 (2013).

64. Van Bilsen K, van Hagen PM, Bastiaans J, *et al.* The neonatal Fc receptor is expressed by human retinal pigment epithelial cells and is downregulated by tumour necrosis factor-alpha. *Br. J. Ophthalmol.* 95(6), 864–868 (2011).

65. Daugherty AL, Mrsny RJ. Formulation and delivery issues for monoclonal antibody therapeutics. *Adv. Drug Deliv. Rev.* 58(5-6), 686–706 (2006).

66. Wadhwa S, Paliwal R, Paliwal SR, Vyas SP. Nanocarriers in Ocular Drug Delivery: An Update Review. *Curr. Pharm. Des.* 15, 2724–2750 (2009).

67. Thrimawithana TR, Young S, Bunt CR, Green C, Alany RG. Drug delivery to the posterior segment of the eye. *Drug Discov. Today*. 16(5-6), 270–277 (2011).

68. Kompella UB, Sundaram S, Raghava S, Escobar ER. Luteinizing hormone-releasing hormone agonist and transferrin functionalizations enhance nanoparticle delivery in a novel bovine ex vivo eye model. *Mol. Vis.* 12, 1185–1198 (2006).

69. Kompella UB, Amrite AC, Pacha Ravi R, Durazo SA. Nanomedicines for back of the eye drug delivery, gene delivery, and imaging. *Prog. Retin. Eye Res.* 36, 172–198 (2013).

70. Chan AC, Carter PJ. Therapeutic Antibodies for Autoimmunity and Inflammation. *Nat. Rev. Immunol.* 10(5), 301–316 (2010).

71. Filpula D. Antibody Engineering and Modification Technologies. *Biomol. Eng.* 24(2), 201–215 (2007).

72. Hanrahan F, Campbell M, Nguyen AT, *et al.* On Further Development of Barrier Modulation as a Technique for Systemic Ocular Drug Delivery [Internet]. In: *Retinal Degenerative Diseases*. LaVail MM, Ash JD, Anderson RE, Hollyfield JG, Grimm C (Eds.). Springer US, Boston, MA, 155–159 (2012) [cited 2013 Sep 11]. Available from: http://www.springerlink.com/index/10.1007/978-1-4614-0631-0_21.

73. Johnson LN, Cashman SM, Kumar-Singh R. Cell-penetrating Peptide for Enhanced Delivery of Nucleic Acids and Drugs to Ocular Tissues Including Retina and Cornea. *Mol. Ther.* 16(1), 107–114 (2007).

74. Mata A, Fleischman AJ, Roy S. Fabrication of multi-layer SU-8 microstructures. *J. Micromechanics Microengineering*. 16(2), 276–284 (2006).

75. Anhoj TA, Jorgensen AM, Zauner DA, Hübner J. The effect of soft bake temperature on the polymerization of SU-8 photoresist. *J. Micromechanics Microengineering*. 16(9), 1819–1824 (2006).

76. Kumar A, Lahiri SS, Singh H. Development of PEGDMA: MAA based hydrogel microparticles for oral insulin delivery. *Int. J. Pharm.* 323(1-2), 117–124 (2006).

77. Ulery BD, Nair LS, Laurencin CT. Biomedical Applications of Biodegradable Polymers. *J. Polym. Sci. Part B Polym. Phys.* 49(12), 832–864 (2011).

78. Peppas NA, Keys KB, Torres-Lugo M, Lowman AM. Poly(ethylene glycol)-containing hydrogels in drug delivery. *J. Controlled Release*. 62(1-2), 81–87 (1999).

79. Leobandung W, Ichikawa H, Fukumori Y, Peppas NA. Monodisperse nanoparticles of poly(ethylene glycol) macromers and N-isopropyl acrylamide for biomedical applications. *J. Appl. Polym. Sci.* 87(10), 1678–1684 (2003).

80. Leobandung W, Ichikawa H, Fukumori Y, Peppas NA. Preparation of stable insulin-loaded nanospheres of poly(ethylene glycol) macromers and N-isopropyl acrylamide. *J. Controlled Release*. 80(1-3), 357–363 (2002).

81. Ainslie KM, Kraning CM, Desai TA. Microfabrication of an asymmetric, multi-layered microdevice for controlled release of orally delivered therapeutics. *Lab. Chip*. 8(7), 1042 (2008).

82. Ainslie KM, Lowe RD, Beaudette TT, Petty L, Bachelder EM, Desai TA. Microfabricated Devices for Enhanced Bioadhesive Drug Delivery: Attachment to and Small-Molecule Release Through a Cell Monolayer Under Flow. *Small*. 5(24), 2857–2863 (2009).

83. Chirra HD, Desai TA. Multi-Reservoir Bioadhesive Microdevices for Independent Rate-Controlled Delivery of Multiple Drugs. *Small*. 8(24), 3839–3846 (2012).

84. Tao SL, Desai TA. Bioadhesive Poly(Methyl Methacrylate) Microdevices for Controlled Drug Delivery. *J. Controlled Release*. 88, 215–228 (2003).

85. Sonoda S. A Protocol for the Culture and Differentiation of Highly Polarized Human Retinal Pigment Epithelial Cells. *Nat. Protoc.* 4(5), 662–673 (2009).

86. Dunn KC. A Human Retinal Pigment Epithelial Cell Line with Differentiated Properties. *Exp. Eye Res.* 62(2), 155–170 (1996).

87. Maminishkis A, Miller SS. Confluent Monolayers of Cultured Human Fetal Retinal Pigment Epithelium Exhibit Morphology and Physiology of Native Tissue. *Invest. Ophthalmol. Vis. Sci.* 47(8), 3612–3624 (2006).

88. Rosenthal R, Günzel D, Finger C, *et al.* The effect of chitosan on transcellular and paracellular mechanisms in the intestinal epithelial barrier. *Biomaterials*. 33(9), 2791–2800 (2012).

89. Mannermaa E, Reinisalo M, Ranta V-P, *et al.* Filter-cultured ARPE-19 cells as outer blood–retinal barrier model. *Eur. J. Pharm. Sci.* 40(4), 289–296 (2010).

90. Deli MA. Potential Use of Tight Junction Modulators to Reversibly Open Membranous Barriers and Improve Drug Delivery. *Biochim. Biophys. Acta*. 1788(4), 892–910 (2009).

91. Kam KR, Walsh LA, Bock SM, *et al.* Nanostructure-Mediated Transport of Biologics Across Epithelial Tissue: Enhancing Permeability via Nanotopography. *Nano Lett.* 13(1), 164–171 (2013).

92. Dalby MJ. Topographically Induced Direct Cell Mechanotransduction. *Med. Eng. Phys.* 27(9), 730–742 (2005).

93. Gunda S. Barriers in Ocular Drug Delivery. In: *Ophthalmology Research: Ocular Transporters in Ophthalmic Diseases and Drug Delivery*. Tombran-Tink J (Ed.). Humana Press, Totowa, 399–413 (2008).

94. Constable PA. P-glycoprotein Expression and Function in the Retinal Pigment Epithelium. In: *Ophthalmology Research: Ocular Transporters in Ophthalmic Diseases and Drug Delivery*. Tombran-Tink J (Ed.). Humana Press, Totowa, 235–253 (2008).

95. Zhang T, Xiang CD, Gale D, Carreiro S, Wu EY, Zhang EY. Drug Transporter and Cytochrome P450 mRNA Expression in Human Ocular Barriers: Implications for Ocular Drug Disposition. *Drug Metab. Dispos.* 36(7), 1300–1307 (2008).

96. Tirucherai GS, Mitra AK. Effect of hydroxypropyl beta cyclodextrin complexation on aqueous solubility, stability, and corneal permeation of acyl ester prodrugs of ganciclovir. *AAPS PharmSciTech*. 4, 1–12 (2003).

97. Kapoor Y, Chauhan A. Ophthalmic delivery of cyclosporine A from brij-97 microemulsion and surfactant-laden p-HEMA hydro- gels. *Int. J. Pharm.* 361, 222–229 (2008).

98. Furrer P, Mayer JM, Plazonnet B, Gurny R. Ocular tolerance of absorption enhancers in opthlamic preparations. *AAPS PharmSciTech*. 4(1), 6–10 (2002).

99. Jain AK, Chalasani KB, Khar RK, Ahmed FJ, Diwan PV. Mucoadhesive multivesicular liposomes as an effective carrier for transmucosal insulin delivery. *J. Drug Target.* 15(6), 417–427 (2007).

100. Aggarwal D, Kaur IP. Improved pharmacodynamics of timolol maleate from a mucoadhesive niosomal ophthalmic drug delivery system. *Int. J. Pharm.* 290(1-2), 155–159 (2005).

101. Borzacchiello A, Ambrosio L, Netti PA, *et al.* Chitosan-based hydrogels: Synthesis and characterization. *J. Mater. Sci. Mater. Med.* 12, 861–864 (2001).

102. Seo T, Ohtake H, Unishi T, lijima T. Permeation of Solutes Through Chemically Modified Chitosan Membranes. *J. Appl. Polym. Sci.* 58, 633–644 (1995).

103. Bhattarai N, Gunn J, Zhang M. Chitosan-based hydrogels for controlled, localized drug delivery⋆. *Adv. Drug Deliv. Rev.* 62(1), 83–99 (2010).

104. Aly AS, Abdel-Mohsen AM, Hebeish A. Innovative multifinishing using chitosan-O-PEG graft copolymer/citric acid aqueous system for preparation of medical textiles. *J. Text. Inst.* 101(1), 76–90 (2010).

105. De la Fuente M, Raviña M, Paolicelli P, Sanchez A, Seijo B, Alonso MJ. Chitosan-based nanostructures: A delivery platform for ocular therapeutics⋆. *Adv. Drug Deliv. Rev.* 62(1), 100–117 (2010).

106. Sogias IA, Williams AC, Khutoryanskiy VV. Why is Chitosan Mucoadhesive? *Biomacromolecules*. 9(7), 1837–1842 (2008).

107. Cao Y, Zhang C, Shen W, Cheng Z, Yu L (Lucy), Ping Q. Poly(N-isopropylacrylamide)–chitosan as thermosensitive in situ gel-forming system for ocular drug delivery. *J. Controlled Release*. 120, 186–194 (2007).

108. Casettari L, Vllasaliu D, Lam JKW, Soliman M, Illum L. Biomedical applications of amino acid-modified chitosans: a review. *Biomaterials*. 33(30), 7565–7583 (2012).

109. Grenha A, Grainger CI, Dailey LA, *et al.* Chitosan nanoparticles are compatible with respiratory epithelial cells in vitro. *Eur. J. Pharm. Sci.* 31, 73–84 (2007).

110. De Campos AM, Sanchez A, Alonso MJ. Chitosan Nanoparticles: A New Vehicle for the Improvement of the Delivery of Drugs to the Ocular Surface. Application to Cyclosporin A. *Int. J. Pharm.* 224, 159–168 (2001).

111. Qu X, Khutoryanskiy VV, Stewart A, *et al.* Carbohydrate-based micelle clusters which enhance hydrophobic drug bioavailability by up to 1 order of magnitude. *Biomacromolecules*. 7(12), 3452–3459 (2006).

112. Alpar H, Somavarapu S, Atuah K, Bramwell V. Biodegradable mucoadhesive particulates for nasal and pulmonary antigen and DNA delivery. *Adv. Drug Deliv. Rev.* 57(3), 411–430 (2005).

113. Schipper NGM, Olsson S, Hoogstraate JA, deBoer AG, Varum KM, Artursson P. Chitosans as Absorption Enhancers for Poorly Absorbable Drugs 2: Mechanism of Absorption Enhancement. *Pharm. Res.* 14(7), 923–929 (1997).

114. Schipper NGM, Varum KM, Stenberg P, Ocklind G, Lennernas H, Artursson P. Chitosans as absorption enhancers of poorly absorbable drugs 3: Influence of mucus on absorption enhancement. *Eur. J. Pharm. Sci.* 8, 335–343 (1999).

115. Artursson P, Lindmark T, Davis SS, Illum L. Effect of Chitosan on the Permeability of Monolayers of Intestinal Epithelial Cells (Caco-2). *Pharm. Res.* 11(9), 1358–1361 (1994).

116. Sadeghi A, Dorkoosh F, Avadi M, *et al.* Permeation enhancer effect of chitosan and chitosan derivatives: Comparison of formulations as soluble polymers and nanoparticulate systems on insulin absorption in Caco-2 cells. *Eur. J. Pharm. Biopharm.* 70(1), 270–278 (2008).

117. De Campos AM, Sanchez A, Gref R, Calvo P, Alonso MJ. The effect of a PEG versus chitosan coating on the interaction of drug colloidal carriers with the ocular mucosa. *Eur. J. Pharm. Sci.* 20(1), 73–81 (2003).

118. Shen L. Tight junctions on the move: molecular mechanisms for epithelial barrier regulation: Molecular mechanisms for tight junction regulation. *Ann. N. Y. Acad. Sci.* 1258(1), 9–18 (2012).

119. Sant S, Tao SL, Fisher OZ, Xu Q, Peppas NA, Khademhosseini A. Microfabrication Technologies for Oral Drug Delivery. *Adv. Drug Deliv. Rev.* 64, 496–507 (2012).

120. Santini JT, Cima MJ, Langer R. A Controlled-release Microchip. *Nature*. 397, 335–338 (1999).

121. Amirouche F, Zhou Y, Johnson T. Current Micropump Technologies and Their Biomedical Applications. *Microsyst. Technol.* 15, 647–666 (2009).

122. Ainslie KM, Desai TA. Microfabricated implants for applications in therapeutic delivery, tissue engineering, and biosensing. *Lab. Chip*. 8(11), 1864 (2008).

123. Herrero-Vanrell R. Microparticles as Drug Delivery Systems for the Back of the Eye. In: *Drug Product Development for the Back of the Eye*. Kompella UB, Edelhauser HF (Eds.). Springer US, Boston, MA, 231–259 (2011).

124. Jennifer S. Wade, Tejal A. Desai. Planar Microdevices Enhance Transport of Large Molecular Weight Molecules Across Retinal Pigment Epithelial Cells. *Biomed. Microdevices*. , 1–10 (2014).

125. Adler AF, Leong KW. Emerging Links Between Surface Nanotechnology and Endocytosis: Impact on Nonviral Gene Delivery. *Nano Today*. 5, 553–569 (2010).

126. Yim EKF, Leong KW. Significance of Synthetic Nanostructures in Dictating Cellular Response. *Nanomedicine Nanotechnol. Biol. Med.* 1(1), 10–21 (2005).

127. Teixeira AI, McKie GA, Foley JD, Bertics PJ, Nealey PF, Murphy CJ. The Effect of Environmental Factors on the Response of Human Corneal Epithelial Cells to Nanoscale Substrate Topography. *Biomaterials*. 27(21), 3945–3954 (2006).

128. Bettinger CJ, Langer R, Borenstein J. Engineering Substrate Topography at the Micro- and Nanoscale to Control Cell Function. *Angew. Chem. Int. Ed.* 48(30), 5406–5415 (2009).

129. Flemming RG, Murphy CJ, Abrams GA, Goodman SL, Nealey PF. Effects of Synthetic Micro- and Nano-structured Surfaces on Cell Behavior. *Biomaterials*. 20, 573–588 (1999).

130. Zauner W, Farrow NA, Haines AMR. In Vitro Uptake of Polystyrene Microspheres: Effect of Particle Size, Cell Line and Cell Density. *J. Controlled Release*. 71(1), 39–51 (2001).

131. Lai SK, Hida K, Man ST, *et al.* Privileged Delivery of Polymer Nanoparticles to the Perinuclear Region of Live Cells via a Non-clathrin, Non-degradative Pathway. *Biomaterials*. 28(18), 2876–2884 (2007).

132. Gratton SEA, Ropp PA, Pohlhaus PD, *et al.* The effect of particle design on cellular internalization pathways. *Proc. Natl. Acad. Sci. U. S. A.* 105(33), 11613–11618 (2008).

133. Decuzzi P, Ferrari M. The Receptor-Mediated Endocytosis of Nonspherical Particles. *Biophys. J.* 94(10), 3790–3797 (2008).

134. Liu G, Li D, Pasumarthy MK, *et al.* Nanoparticles of Compacted DNA Transfect Postmitotic Cells. *J. Biol. Chem.* 278, 32578–32586 (2003).

135. Jongho Lee, Ronald S. Fearing. Contact Self-Cleaning of Synthetic Gecko Adhesive from Polymer Microfibers. *Langmuir*. 24, 10587–10591 (2008).

136. Jongho Lee, Carmel Majidi, Bryan Schubert, Ronald S. Fearing. Sliding-induced Adhesion of Stiff Polymer Microfibre Arrays. I. Macroscale Behaviour. *J. R. Soc. Interface*. 5(25), 835–844 (2008).

137. Veurink M, Stella C, Tabatabay C, Pournaras CJ, Gurny R. Association of Ranibizumab (Lucentis) or Bevacizumab (Avastin) with dexamethasone and triamcinolone acetonide: An in vitro stability assessment. *Eur. J. Pharm. Biopharm.* 78(2), 271–277 (2011).

138. Kenneth J. Livak, Thomas D. Schmittgen. Analysis of Relative Gene Expression Data Using Real- Time Quantitative PCR and the 2(-Delta Delta C(T)) Method. *Methods*. 25(4), 402–408 (2001).

139. Peng S, Rao VS, Adelman RA, Rizzolo LJ. Claudin-19 and the Barrier Properties of the Human Retinal Pigment Epithelium. *Invest. Ophthalmol. Vis. Sci.* 52(3), 1392–1403 (2011).

140. Findley MK, Koval M. Regulation and roles for claudin-family tight junction proteins. *Int. Union Biochem. Mol. Biol. Life*. 61(4), 431–437 (2009).

141. Mayssa Attar, Jie Shen. The Emerging Significance of Drug Transporters and Metabolizing Enzymes to Ophthalmic Drug Design. In: *Ophthalmology Research: Ocular Transporters in Ophthalmic Diseases and Drug Delivery*. J. Tombran-Tink (Ed.). Humana Press, Totowa, 375–397 (2008).

142. Lawrence J. Rizzolo. Glucose Transporters in Retinal Pigment Epithelium Development. In: *Ophthalmology Research: Ocular Transporters in Ophthalmic Diseases and Drug Delivery*. J. Tombran-Tink (Ed.). Humana Press, Totowa, 185–199 (2008).

143. Nagesh Bandi, Uday B. Kompella. Budesonide reduces multidrug resistance-associated protein 1 expression in an airway epithelial cell line (Calu-1). *Eur. J. Pharmacol.* 437, 9–17 (2002).

144. Yalcin Ozkan, Niyazi Yilmaz, SIbel A. Ozkan, Inci Biryol. High-performance liquid chromatographic analysis of verapamil and its application to determination in tablet dosage forms and to drug dissolution studies. *Il Farm.* 55, 376–382 (2000).

145. Douglas W. Low, Roger G. Deeley, Susan P. C. Cole. Verapamil Stimulates Glutathione Transport by the 190-kDa Multidrug Resistance Protein 1 (MRP1). *J. Pharmacol. Exp. Ther.* 293(2), 530–538 (2000).

146. Hideo Ueda, Yoshihide Horibe, Kwang-Jin Kim, Vincent H. L. Lee. Functional Characterization of Organic Cation Drug Transport in the Pigmented Rabbit Conjunctiva. *Invest. Ophthalmol. Vis. Sci.* 41(3), 870–876 (2000).

147. Scott W. Grimm, Heidi J. Einolf, Steven D. Hall, *et al.* The Conduct of in Vitro Studies to Address Time-Dependent Inhibition of Drug-Metabolizing Enzymes: A Perspective of the Pharmaceutical Research and Manufacturers of America. *Drug Metab. Dispos.* 37(7), 1355–1370 (2009).

148. Yoshiyuki Kubo, Yusuke Kusagawa, Masanori Tachikawa, Shin-ichi Akanuma, Ken-ichi Hosoya. Involvement of a Novel Organic Cation Transporter in Verapamil Transport Across the Inner Blood-Retinal Barrier. *Pharm. Res.* 30, 847–856 (2013).

Supplementary Material

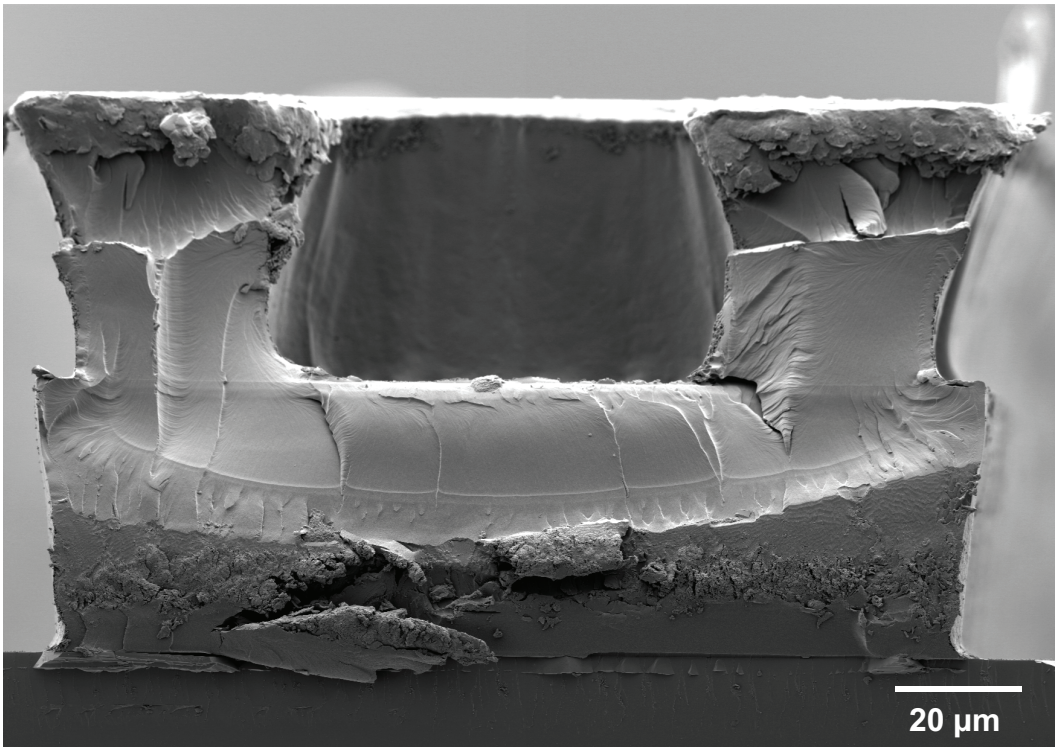

Figure 2.S1 Planar Device SEM. Scanning electron microscopy cross-section of a single planar microdevice with an empty reservoir.

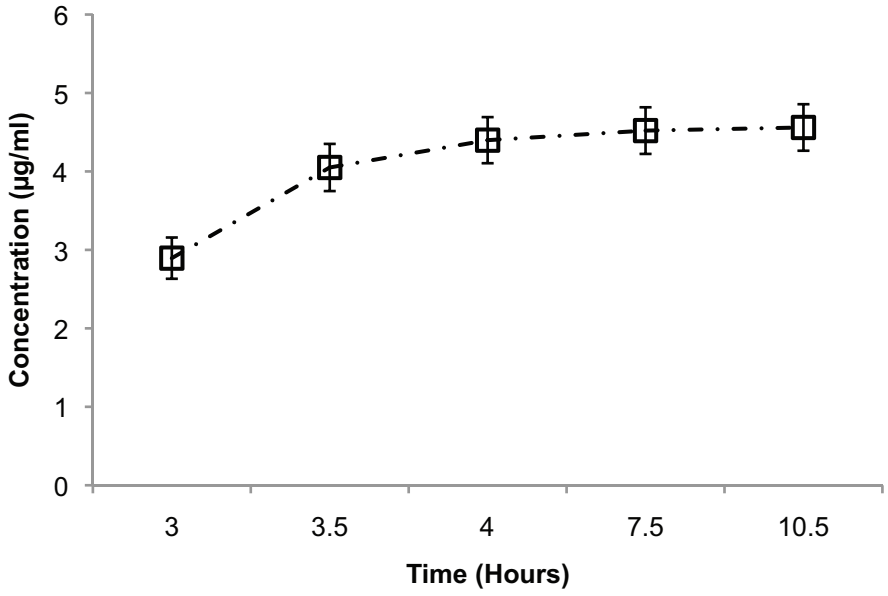

Figure 2.S2 FITC Dextran Elution. Elution of FITC dextran from SU-8/PEGDMA planar microdevices over 10.5 hours. All experiments were conducted in PBS at 37°C. Error bars represent the mean +/- standard deviation.

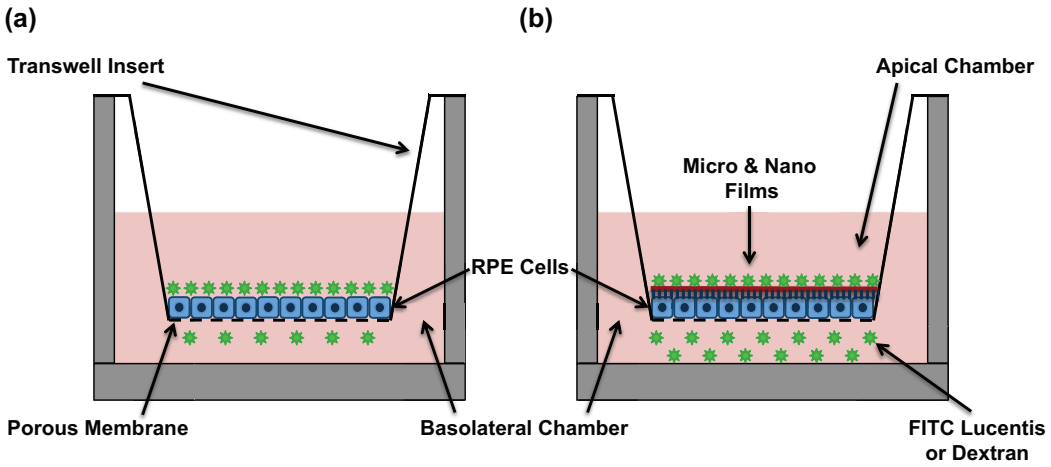

Figure 4.S1 Permeability Studies Experimental Setup. (a) Schematic representation of a transwell insert with bolus drug being deposited in the apical chamber. (b) Schematic representation of supermicro, micro or nanofiber films placed in contact with human fetal retinal pigment epithelial cells (hfRPE) in the presence of a FITC conjugated macromolecule.

Publishing Agreement

It is the policy of the University to encourage the distribution of all theses, dissertations, and manuscripts. Copies of all UCSF theses, dissertations, and manuscripts will be routed to the library via the Graduate Division. The library will make all theses, dissertations, and manuscripts accessible to the public and will preserve these to the best of their abilities, in perpetuity.

Please sign the following statement:

I hereby grant permission to the Graduate Division of the University of California, San Francisco to release copies of my thesis, dissertation, or manuscript to the Campus Library to provide access and preservation, in whole or in part, in perpetuity.

Jennifer S Wade
Author Signature

07/04/14
Date